Positive-Net-Damping Stability Criterion in Grid-Connected VSC Systems

Journal:	*Journal of Emerging and Selected Topics in Power Electronics*
Manuscript ID	JESTPE-2017-01-0027.R1
Manuscript Type:	Special Issue on Power Electronics & Systems: Modeling, Analysis, Control, and Stability
Date Submitted by the Author:	n/a
Complete List of Authors:	Sainz, Luis; Universitat Politecnica de Catalunya, Electrical Engineering Cheah-Mane, Marc; Cardiff University, School of Engineering Monjo, Lluis; Univ. Jaume I, Dep. of Industrial and Design System Engineering Liang, Jun; Cardiff University, School of Engineering Oriol, Gomis-Bellmunt; CITCEA-UPC,
Keywords:	Stability analysis, Resonance, Damping, Converters

Positive-Net-Damping Stability Criterion in Grid-Connected VSC Systems

L. Sainz, M. Cheah-Mane, Ll. Monjo, J. Liang, O. Gomis-Bellmunt

***Abstract*- Resonance instabilities in power systems can be assessed with the positive-net-damping stability criterion. This criterion is a review of the complex torque coefficients method but it does not provide the frequency of the closed-loop oscillatory modes. This paper presents an alternative approach of the positive-net-damping stability criterion for electrical resonance instability assessment. In this approach, resonance instabilities are identified in feedback systems derived from impedance-based equivalent circuits. The proposed approach allows characterizing the frequency of closed-loop oscillatory modes and identifying the physical and control parameters of the system that increase or reduce the damping of these modes. The extension of the proposed approach to study the stability of Single-Input Single-Output and Multiple-Input Multiple-Output feedback systems is analyzed and the approach is also compared with other stability methods in the literature. An example of an offshore wind power plant illustrates the theoretical study and compares the proposed approach with different methods for stability assessment. Time-domain simulations in PSCAD/EMTDC are shown to validate the stability study.**

***Index Terms*— Electrical resonance, voltage stability, voltage source converters.**

I. Introduction

Grid-connected voltage source converters (VSCs) are widely used in renewable energy conversion systems (variable speed wind turbines and photovoltaics) and energy storage systems to improve controllability in power systems (e.g., microgrids [1] and wind power plants (WPPs) [2], [3]). However, resonance instabilities can appear in poorly damped power systems due to interaction between VSC control and the grid. In general, these resonance instabilities can be classified in two categories [4]: (i) Harmonic resonance instabilities which approximately range from 0.75 to 2 kHz and are caused by negative dampings due to VSC time delay and current control dynamics. (ii) Near-synchronous resonance instabilities which approximately range from 50 to 300 Hz and are caused by negative dampings due to current control dynamics and outer loop controls. The harmonic resonance instabilities are reported in different grid-connected VSC applications such as single-phase ac traction systems [6] and WPPs [7]. A number of methods to analyze resonance stability are reported in the literature [4], [8] – [19]. A good method is expected to have the following characteristics: (i) be simple to evaluate and compute, (ii) offer the possibility to assess stability from measurements and not requiring detailed knowledge of the system, (iii) provide enough information to understand physically instabilities and their causes and (iv) characterize the frequency of closed-loop unstable oscillatory modes.

The state space eigenvalue analysis (or closed-loop root study) and frequency domain methods are used to analyze the impact of system and control parameters on stability [8] – [13]. The Nyquist criterion and the phase and gain margin from the Bode diagram are the most used frequency domain methods to determine stability [9] – [13]. Other frequency domain methods are based on the impedance characterization of the system which allows considering the individual contribution that source and load subsystems have on the closed-loop stability [4], [9] – [20]. The passivity-based method ensures that a closed-loop system is stable if the real part of each subsystem is nonnegative for all frequencies [4], [13], [14]. This method imposes passivity on all system elements to achieve stability but the non-passivity of a subsystem does not necessarily mean that system is unstable. On the other hand, the following methods derived from the Nyquist criterion consider the stability contribution of each subsystem even when they are not passive:

- The impedance-based stability criterion [10] – [12] evaluates the phase of the open-loop functions at frequencies where the open-loop magnitudes intersect.
- The positive-net-damping stability criterion [19], [20] evaluates the net damping of the system at frequencies where the loop gain is greater than 1 as well as at frequencies of each open-loop resonance. This criterion is proposed by [20] to review the complex torque coefficients method [15] – [18] which is applied to study subsynchronous torsional interactions of turbine-generator sets [15], [16].

The impedance-based stability criterion provides information on the frequency of the closed-loop oscillatory modes from the frequency of the open-loop magnitude intersection while the positive-net-damping stability criterion only provides information on the frequency range of these oscillatory modes. The positive-net-damping stability criterion focuses on the net damping (i.e., the sum of the source and load resistances or conductances) while the impedance-based stability criterion focuses on the phase margin of the source and load impedance ratio. A recent study based on the complex torque coefficients method investigates near-synchronous resonance instabilities in grid-connected VSC systems from the analysis of the damping at the closed-loop oscillatory modes [21]. The damping is also used in [22] to study stability in weak grid-connected VSC systems. The conclusions in [22] are graphically obtained from the damping evaluation with the phase of the system transfer function instead with the real part of this function.

This paper presents and mathematically demonstrates an alternative approach to the positive-net-damping stability criterion for studying harmonic resonance instabilities in grid-connected VSC systems. This approach meets the advantages of the impedance-based stability criterion (it allows characterizing the frequency of closed-loop oscillatory modes) and the positive-net-damping stability criterion (it allows identifying the physical and control parameters of the system that increase or reduce the damping of the closed-loop oscillatory modes). The approach is also compared analytically and numerically with other methods in the

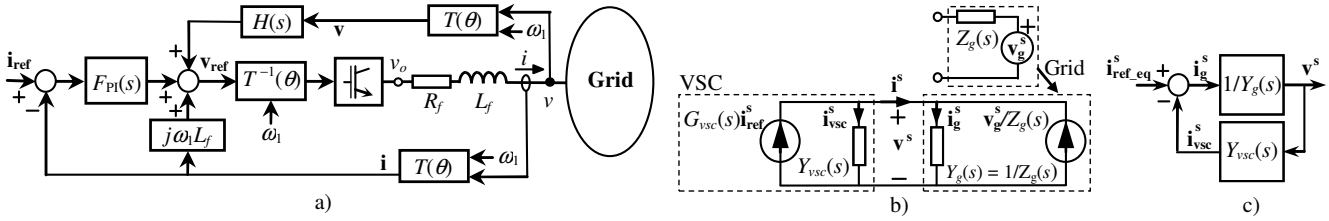

Fig. 1. Grid-connected VSC system modeling: a) Grid-connected VSC system. b) Equivalent circuit. c) Closed-loop system.

literature. Moreover, the extension of the proposed approach to assess the stability of Single-Input Single-Output (SISO) and Multiple-Input Multiple-Output (MIMO) feedback systems derived from impedance-based equivalent circuits is discussed. An example of an offshore WPP illustrates the application of this criterion. The analytical and numerical results are validated by time-domain simulations in PSCAD/EMTDC.

II. Grid-Connected VSC Modeling

Fig. 1(a) presents a grid-connected VSC system where the grid can include the effect of other VSCs. The *dq*-frame PI-based current control of the VSC is explicitly illustrated with bold letters denoting the complex space vectors (i.e., $\mathbf{x} = x_d + j \cdot x_q$) [13]. These space vectors are related to the grid components of angular fundamental (synchronous) frequency $\omega_1 = 2\pi \cdot f_1$ by means of the corresponding transfer matrices. It must be noted that the converter model in this Section only represents the inner current control loop because the outers loops (e.g., the phase-locked loop, PLL, and the direct-voltage controller, DVC) do not affect harmonic resonance instabilities in the 0.75 kHz to 2 kHz frequency range due to their low bandwidths [4], [5]. It can be observed that the transfer matrices of the VSC models in [14] become the common diagonal matrices of the VSC inner current control loop for frequencies greater than the low bandwidths of the outer control loops. This assumption allows a VSC symmetrical model to be obtained which can be characterised with complex impedances or admittances. If outer loops are included, the system becomes nonlinear and VSCs must be represented by real vectors and transfer matrices leading to a two-dimensional MIMO model [23].

A. VSC model

The VSC current control model is obtained from the voltage balance across the converter filter,

$$(R_f + L_f s + jL_f \omega_1)\mathbf{i} + \mathbf{v} = \mathbf{v_o}, \tag{1}$$

and the control law

$$\mathbf{v_{ref}} = F_{PI}(s)\left(\mathbf{i_{ref}} - \mathbf{i}\right) + jL_f \omega_1 \mathbf{i} + H(s)\mathbf{v}, \tag{2}$$

where $\mathbf{v}$ and $\mathbf{i}$ are the grid voltage and current, $\mathbf{v_o}$ is the converter output voltage, $\mathbf{v_{ref}}$ and $\mathbf{i_{ref}}$ are the converter voltage and current

reference and $F_{PI}(s)$ and $H(s)$ are the transfer functions of the feedback PI controller and the grid voltage feedforward low-pass filter included in the control,

$$F_{PI}(s) = k_p + \frac{k_i}{s} \qquad H(s) = \frac{\alpha_f}{s + \alpha_f}, \tag{3}$$

with k_p and k_i being the PI controller proportional and integral gains, respectively, and α_f (or $f_f = \alpha_f/(2\pi)$) the low-pass filter bandwidth. Based on [14], the control design results in $k_p = \alpha_c L_f$ and $k_i = \alpha_c R_f$ where α_c is the closed current control loop bandwidth which should verify $\alpha_c \leq 0.2 \cdot (2\pi f_{sw})$ with f_{sw} being the converter switching frequency. The selection of the low-pass filter bandwidth is a compromise between the stability of the VSC output and the whole system stability [2], [13], [14], [22]. A small vale of this bandwidth is used to keep as narrow as possible the VSC non-passivity region and improve the VSC stability. On the other hand, a large value is required to improve dynamics during fast transients due to grid disturbances which affect stability of VSC terminal voltage. The recommended low-pass filter bandwidth is $\alpha_f \leq 0.1\alpha_c$ for normal-mode operation and $\alpha_f \geq \alpha_c$ for transient-mode operation [14]. If the VSC connects to a stiff bus, the feedforward low-pass filter design $\alpha_f \leq 0.1 \cdot \alpha_c$ ensures steady converter current output [14]. If VSC connects to a weak grid, the feedforward low-pass filter design $\alpha_f \geq \alpha_c$ ensures terminal voltage dynamics stability and avoid that voltage becomes unstable in case of grid disturbances [2], [22].

The voltage $\mathbf{v_o}$ generated by the VSC is related to the converter-voltage reference $\mathbf{v_{ref}}$ considering the VSC time delay T_d as follows [4]:

$$\mathbf{v_o} = e^{-sT_d}\,\mathbf{v_{ref}}. \tag{4}$$

This time delay is caused by the computation and the switching process and is approximately given by $T_d \approx 1.5T_s$ with $T_s = 1/f_s$ and f_s being the converter sampling frequency which is assumed twice the converter switching frequency [4]. Considering (4), the following relation between the grid voltage and current is obtained from (1) and (2):

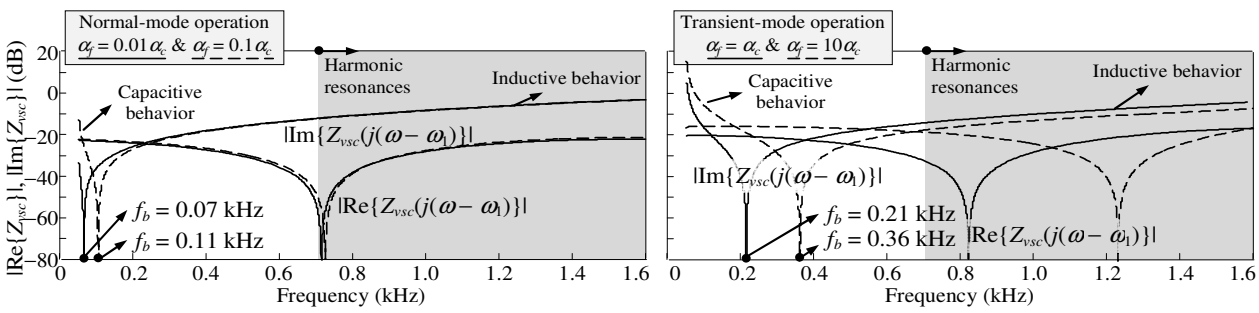

Fig. 2. Study of the VSC equivalent impedance beahavior.

$$\mathbf{i} = G_{vsc}(s)\mathbf{i}_{\mathbf{ref}} - Y_{vsc}(s)\mathbf{v}, \tag{5}$$

with

$$G_{vsc}(s) = \frac{e^{-sT_d} F_{\mathrm{PI}}(s)}{R_f + L_f s + jL_f\omega_1 + e^{-sT_d}(F_{\mathrm{PI}}(s) - jL_f\omega_1)} \qquad Y_{vsc}(s) = \frac{1 - e^{-sT_d} H(s)}{R_f + L_f s + jL_f\omega_1 + e^{-sT_d}(F_{\mathrm{PI}}(s) - jL_f\omega_1)}, \tag{6}$$

where $G_{vsc}(s)$ is the closed-loop transfer function and $Y_{vsc}(s)$ is the equivalent admittance of the VSC.

Fig. 2 illustrates the frequency response of the positive-sequence VSC equivalent impedance in $\alpha\beta$-frame $Z_{vsc}(s) = 1/Y_{vsc}(s)$ (6) with $s = j(\omega - \omega_1)$ [11] for the parameter values in Table I and four values of the low-pass filter bandwidth corresponding to normal-mode operation ($\alpha_f = 0.01\alpha_c$ and $\alpha_f = 0.1\alpha_c$) and transient-mode operation ($\alpha_f = \alpha_c$ and $\alpha_f = 10\alpha_c$). The frequency range of the harmonic resonance frequencies is also indicated in grey color [4]. It can be observed that for usual values of VSC parameters the VSC equivalent impedance presents a capacitive and an inductive behavior below and above the boundary frequency f_b [12]. It can also be observed that the behavior above the boundary frequency f_b is mainly inductive due to the low contribution of the VSC resistive behavior. Thus, the VSC equivalent impedance at harmonic resonance instability frequencies is mainly inductive [12] because these frequencies are greater than the boundary frequency [4], [5].

B. Grid-connected VSC model

Considering the above VSC model, the impedance-based equivalent circuit of the grid-connected VSC system is shown in Fig. 1(b), where the VSC is represented as a current source in parallel with the equivalent VSC admittance, and the grid (characterized as stiff – or ideal – voltage source $\mathbf{v_g}$ in series with the grid equivalent impedance $Z_g(s)$) is also modeled as a current source $\mathbf{v_g}/Z_g(s)$ in parallel with the grid equivalent admittance $Y_g(s) = 1/Z_g(s)$. The resistive elements of the ac grids may be usually neglected compared to the reactive elements and the impedance $Z_g(s)$ is commonly characterized by reactances in harmonic resonance studies [12], [14], [21]. It must be noted that the grid and VSC transfer functions are in phase and *dq* coordinates, respectively, and they must be in the same frame in Fig. 1(b) to assess stability studies. For that, both transfer functions are expressed in $\alpha\beta$ coordinates with bold letters denoting the space vectors and superscript **s** denoting the $\alpha\beta$-

TABLE I. VSC PARAMETERS

Switching frequency	f_{sw}	2.5 kHz
Filter resistance	R_f	0.0075 mΩ
Filter inductance	L_f	0.07 mH
Filter capacitance	C_f	1150 µF
Closed-loop time constant	$d\,\mathrm{resist}_a n$1 ms	1 ms
Voltage filter bandwidth	$f_f = \alpha_f/2\pi$	1.25 kHz
PI control proportional gain	$k_p = \alpha_c \cdot L_f$	0.07
PI control integral gain	$k_i = \alpha_c \cdot R_f$	0.0075
Time delay	$T_d = 1.5/f_s$	0.3 ms

frame (i.e., $\mathbf{x}^s = x_\alpha + j \cdot x_\beta$). The VSC closed-loop transfer function and equivalent admittance in (6) are transformed from dq coordinates to $\alpha\beta$ coordinates by means of the frequency translation $s \to s - j\omega_1$ and the grid transfer function in phase coordinates is the same as in $\alpha\beta$ coordinates [18], [23].

The impedance-based equivalent circuit in Fig. 1(b) can also be represented as the closed-loop system in Fig. 1(c), [10], [11], which is obtained from the transfer function between the sources and the grid voltage v (or current i) as follows:

$$\begin{aligned} \mathbf{v}^s &= Z_t(s)\mathbf{i}^s_{\text{ref\_eq}} \\ \mathbf{i}^s_{\text{ref\_eq}} &= G_{vsc}(s)\mathbf{i}^s_{\text{ref}} + \frac{\mathbf{v}^s_{\mathbf{g}}}{Z_g(s)} \qquad Z_t(s) = \frac{1}{Y_g(s)+Y_{vsc}(s)} = \frac{1/Y_g(s)}{1+Y_{vsc}(s)/Y_g(s)}, \end{aligned} \tag{7}$$

and it can be represented by the transfer function

$$F(s) = \frac{M(s)}{1+L(s)} \qquad L(s) = M(s)N(s), \tag{8}$$

where $L(s)$ is the loop transfer function and

$$M(s) = \frac{1}{Y_g(s)} \qquad N(s) = Y_{vsc}(s), \tag{9}$$

are the open-loop and feedback transfer functions, respectively.

If the outer loops are considered in the VSC characterization, the VSC model in $\alpha\beta$- or dq-frame is a two-dimensional MIMO system because VSC must be represented by real vectors and transfer matrices. The impedance-based representation of the grid-connected VSC system (8) becomes [23],

$$F(s) = \left[I + L(s)\right]^{-1} Z_g(s) \qquad L(s) = Y_{vsc}(s)Z_g(s), \tag{10}$$

where, considering $\alpha\beta$-frame,

$$\begin{aligned} Y^s_{vsc}(s) &= \begin{bmatrix} Y_{vsc\_\alpha\alpha}(s) & Y_{vsc\_\alpha\beta}(s) \\ Y_{vsc\_\beta\alpha}(s) & Y_{vsc\_\beta\beta}(s) \end{bmatrix} \qquad Z^s_g(s) = \begin{bmatrix} Z_{g\_\alpha\alpha}(s) & 0 \\ 0 & Z_{g\_\beta\beta}(s) \end{bmatrix} \\ L^s(s) &= \begin{bmatrix} L_{\alpha\alpha}(s) & L_{\alpha\beta}(s) \\ L_{\beta\alpha}(s) & L_{\beta\beta}(s) \end{bmatrix} = \begin{bmatrix} Y_{vsc\_\alpha\alpha}(s)Z_{g\_\alpha\alpha}(s) & Y_{vsc\_\alpha\beta}(s)Z_{g\_\beta\beta}(s) \\ Y_{vsc\_\beta\alpha}(s)Z_{g\_\alpha\alpha}(s) & Y_{vsc\_\beta\beta}(s)Z_{g\_\beta\beta}(s) \end{bmatrix}. \end{aligned} \tag{11}$$

III. Passivity and Stability of Grid-Connected VSCs

Harmonic resonance can destabilize grid-connected VSCs due to VSC non-passivity [4], [13]. These instabilities can be investigated from the impedance-based closed-loop system in Fig. 1(c). This impedance-based system allows stability to be

assessed from a frequency-domain approach. Frequency domain methods for stability assessment must analyze the system response for positive- ($s = j\omega,\ \omega > 0$) and negative- ($s = -j\omega,\ \omega > 0$) sequence because the frequency response of $F(j\omega)$ and $F(-j\omega),\ \omega > 0$ may not be equal since $F^*(j\omega)$ may be different from $F(-j\omega)$ (see example in Appendix A) [11], [23]. Passivity and stability analysis can be considered in the study.

A. *Passivity*

According to [13], the closed-loop system defined by $F(s)$ in (8) is passive if $M(s)$ and $N(s)$ are passive (i.e., $M(s)$ and $N(s)$ are stable, $\mathrm{Re}\{M(j\omega)\} \geq 0,\ -\infty < \omega < \infty$, and $\mathrm{Re}\{N(j\omega)\} \geq 0,\ -\infty < \omega < \infty$) because it is verified that $F(s)$ is also passive, i.e.,

- $F(s)$ is stable since $-\pi \leq \arg\{L(j\omega)\} \leq \pi,\ -\infty < \omega < \infty$, and therefore the Nyquist criterion is satisfied.
- $\mathrm{Re}\{F(j\omega)\} \geq 0,\ -\infty < \omega < \infty$.

B. *Stability*

The passivity condition of grid-connected VSC systems can be reduced when only their stability is analyzed because $F(s)$ in (8) is not necessarily unstable if $M(s)$ and $N(s)$ are not passive. For these cases, system stability can be studied in different ways:

- Analyzing the state-space eigenvalues, the poles of $F(s)$ or the roots of $1 + L(s) = Y_g(s) + Y_{vsc}(s) = 0$.
- Applying the Nyquist criterion to the loop transfer function $L(s)$ for $s = j\omega,\ -\infty < \omega < \infty$ or the phase and gain margin conditions from the Bode diagram to the loop transfer function $L(s)$ for $s = \pm j\omega,\ \omega > 0$ [9] – [13], [21].
- Applying the impedance-based stability criterion. This criterion evaluates the difference between the phase of the VSC and grid admittances $Y_{vsc}(\pm j\omega),\ Y_{grid}(\pm j\omega),\ \omega > 0$ at frequencies where their magnitudes intersect [10] – [12].
- Applying the positive-net-damping stability criterion in [19], [20] or the alternative approach to this criterion presented in the paper. These criteria evaluate the net-damping contribution of grid and VSC admittances at resonance frequencies (see the next Section).

The impedance-based and positive-net-damping stability criteria allow analyzing stability considering the contribution of each system admittance.

IV. Positive-Net-Damping Stability Criterion

The positive-net-damping stability criterion is proposed and strictly demonstrated for stability studies of SISO systems in [18] – [20]. It is applied to subsynchronous torsional interactions in [18] and two-terminal VSC-HVDC systems in [20]. Although this criterion is a powerful tool for stability assessment, it does not characterize the frequency of the closed-loop unstable oscillatory modes. A reformulation of the positive-net-damping criterion for harmonic resonance instabilities of SISO feedback systems is

presented to address the above drawback. This is analytically demonstrated in the frequency- and *s*-domains.

A. Study in the frequency-domain

Considering that $M(s)$ and $N(s)$ are both stable, the closed-loop system defined by $F(s)$ in (8) is asymptotically stable if the Nyquist curve of the loop transfer function $L(s) = M(s)N(s)$ for $s = j\omega$, $-\infty < \omega < \infty$ does not encircle the -1 point. In the literature, the analysis of the Nyquist criterion is conducted from the gain margin condition to prove the positive-net-damping stability criterion for SISO feedback systems [19]. The alternative approach of the positive-net-damping stability criterion in the paper is based on the impedance-based stability criterion [10] – [12] which evaluates the phase margin condition of the Nyquist criterion. In the following Subsections, the study of the positive-net-damping stability criterion based on the gain and phase margin conditions are presented. Although these criteria must be evaluated for the positive- ($s = j\omega$, $\omega > 0$) and negative- ($s = -j\omega$, $\omega > 0$) sequence [11], [12], [23], the study below is made considering only the positive sequence for sake of simplicity in the exposition. Nevertheless, the conclusions must also be applied for the negative-sequence.

1) Positive-net-damping stability criterion from the gain margin

The analysis of the Nyquist criterion from the gain margin means that $L(s)$ must verify two necessary conditions at the same angular frequency ω:

$$\mathrm{Im}\{M(j\omega)N(j\omega)\} = 0, \tag{12}$$

$$M(j\omega)N(j\omega) > -1. \tag{13}$$

Note that the $M(j\omega)N(j\omega)$ value at the frequency of (12) is the cross point of the Nyquist curve $L(s)$ with the real axis which should be on the right hand side of -1 for stability assessment, i.e. (13) may be hold. The above conditions lead to the theorem proposed in [19], which states that the closed-loop system $F(s)$ in (8) is asymptotically stable if the net damping of the system is positive, i.e., $\mathrm{Re}\{Y_g(j\omega) + Y_{vsc}(j\omega)\} > 0$, at the angular frequencies for which $\mathrm{Im}\{M(j\omega)N(j\omega)\} = 0$ (i.e., at the angular frequencies where the Nyquist curve intersects with the real axis). This theorem allows system stability to be accurately assessed. Moreover, the positive-net-damping stability criterion is derived from the above theorem to avoid solving (12). This criterion states that the closed-loop system is asymptotically stable if the net damping of the system is positive for low frequencies where $|M(j\omega)N(j\omega)| > 1$, as well as in the neighborhood of each open-loop $M(j\omega)$ and $N(j\omega)$ resonance (i.e., in the neighborhood of the grid or VSC resonance). The conditions that replace the equation of the Nyquist curve intersection with the real axis in (12) are based on [18] and provide reasonable possibilities of stability for SISO feedback systems. However, they do not provide a clear relation between harmonic resonances of the grid-connected VSC system and stability (see Section V). The application of this criterion is not limited to an impedance representation of the grid and VSC as presented in [20].

2) Positive-net-damping stability criterion from the phase margin

The analysis of the Nyquist criterion from the phase margin means that $L(s)$ must verify the following two necessary conditions at the same angular frequency ω [9] – [11]:

$$\left|M(j\omega)N(j\omega)\right| = 1, \tag{14}$$

$$-\pi \le \arg\left\{M(j\omega)N(j\omega)\right\} \le \pi. \tag{15}$$

Considering the frequency response of the positive-sequence grid and the VSC admittances in Fig. 1(b) as follows:

$$Y_g(j\omega) = \frac{1}{Z_g(j\omega)} = G_g(\omega) + jB_g(\omega) \qquad Y_{vsc}(j\omega) = G_{vsc}(\omega) + jB_{vsc}(\omega), \tag{16}$$

the loop transfer function $L(s) = M(s)N(s)$ can be written as the following expression:

$$L(j\omega) = M(j\omega)N(j\omega) = \frac{G_{vsc}(\omega) + jB_{vsc}(\omega)}{G_g(\omega) + jB_g(\omega)}, \tag{17}$$

which combines the stability conditions with the admittances of the equivalent circuit in Fig. 1(b).

The first phase margin condition (14) can be expressed as

$$\left|L(j\omega)\right| = \frac{\left|Y_{vsc}(j\omega)\right|}{\left|Y_g(j\omega)\right|} = \frac{\sqrt{G_{vsc}^2(\omega) + B_{vsc}^2(\omega)}}{\sqrt{G_g^2(\omega) + B_g^2(\omega)}} = 1 \quad \Rightarrow \quad G_g^2(\omega) + B_g^2(\omega) = G_{vsc}^2(\omega) + B_{vsc}^2(\omega). \tag{18}$$

Considering the main reactive (inductive or capacitive) nature of the grid and VSCs at harmonic resonances (see Section II), $G_i(\omega) << B_i(\omega)$ for $i = g, vsc$ and (18) can be approximated as

$$B_g(\omega) = \pm B_{vsc}(\omega). \tag{19}$$

The parallel resonance observed from the VSC current source in Fig. 1(b), neglecting the conductances $G_g(\omega)$ and $G_{vsc}(\omega)$ with respect to the susceptances $B_g(\omega)$ and $B_{vsc}(\omega)$ due to the main capacitive and inductive nature of the grid and VSCs at the harmonic resonances, can be expressed as

$$\mathrm{Im}\left\{Y_g(j\omega) + Y_{vsc}(j\omega)\right\} \approx 0 \quad \Rightarrow \quad B_g(\omega) \approx -B_{vsc}(\omega), \tag{20}$$

which matches with the negative sign expression in (19). Thus, this parallel resonance is a particular case of the stability condition $|M(j\omega)N(j\omega)| = 1$. The parallel resonance can also be obtained from the parallel equivalent impedance $Z_i(j\omega)$ (7). Most resonance studies in grid-connected VSC systems consider VSC as an ideal current source and impose $B_g(\omega) = 0$ to characterize

parallel resonance [3]. However, Section VI shows that this approximation can provide inaccurate results.

The second phase margin condition (15) can be expressed in terms of the imaginary part of $M(j\omega)N(j\omega)$ in the following two cases

- Case #1: If $d\left|L(j\omega)\right|/d\omega > 0$,

$$0 < \arg\{L(j\omega)\} < \pi: \; G_g(\omega)B_{vsc}(\omega) - G_{vsc}(\omega)B_g(\omega) > 0. \tag{21}$$

- Case #2: If $d\left|L(j\omega)\right|/d\omega < 0$,

$$-\pi < \arg\{L(j\omega)\} < 0: \; G_g(\omega)B_{vsc}(\omega) - G_{vsc}(\omega)B_g(\omega) < 0. \tag{22}$$

Imposing the parallel resonance relation (20), (21) and (22) can be rewritten as

$$\begin{aligned} &\text{Case \#1: } d\left|L(j\omega)\right|/d\omega > 0 \;\Rightarrow\; B_{vsc}(\omega)\left(G_g(\omega) + G_{vsc}(\omega)\right) > 0 \\ &\text{Case \#2: } d\left|L(j\omega)\right|/d\omega < 0 \;\Rightarrow\; B_{vsc}(\omega)\left(G_g(\omega) + G_{vsc}(\omega)\right) < 0. \end{aligned} \tag{23}$$

As demonstrated in the Appendix B, Case #1 is produced by inductive grid and capacitive VSC admittances (i.e., $B_g < 0$ and $B_{vsc} > 0$, respectively) and Case #2 is produced by capacitive grid and inductive VSC admittances (i.e., $B_g > 0$ and $B_{vsc} < 0$, respectively). Therefore, the condition in (23) is always satisfied if

$$G(\omega) = G_g(\omega) + G_{vsc}(\omega) > 0, \tag{24}$$

where the conductance $G(\omega)$ corresponds to the net-damping of the grid-connected VSC, the conductance $G_g(\omega)$ is the grid damping and the conductance $G_{vsc}(\omega)$ is the VSC damping. Therefore, grid-connected VSC systems are asymptotically stable if (24) holds at the angular frequency ω for which (20) holds. This result demonstrates an alternative approach for the positive-net-damping stability criterion based on the gain margin condition [19]: grid-connected VSC systems are asymptotically stable if net damping $G(\omega)$ is positive in a neighborhood of parallel resonances between the grid and VSC impedance. This demonstration can be extended to SISO feedback systems derived from impedance-based equivalent circuits if the equivalent resistances of the circuit are not significant compared to the reactances (i.e., the equivalent impedances of the circuit are mainly inductive or capacitive). Although the criterion is demonstrated for the positive-sequence ($s = j\omega$, $\omega > 0$), it must also applied for the negative-sequence ($s = -j\omega$, $\omega > 0$). Note that, although the VSC could be considered as an ideal current source for parallel resonance determination, its representation as a Norton equivalent source is necessary to consider the VSC control influence on net damping, and therefore on electrical resonance instabilities. If the VSC is connected to a passive grid, grid damping $G_g(\omega)$ is always positive and the converter control could be designed only by considering the passivity conditions of the VSC equivalent

admittance [4], [13], [14].

If the outer loops are considered in the VSC characterization, the VSC model in $\alpha\beta$- or dq-frame is a two-dimensional MIMO system (10) and the stability must be analyzed using the generalized Nyquist method (GNC) which extends the traditional Nyquist criterion to the eigenloci of the system return-ratio matrix (i.e., to the Nyquist curves of the eigenvalues of the loop gain transfer matrix) [9], [23]. These eigenvalues are obtained from the loop transfer function $L^s(s)$ (11),

$$\begin{aligned} &\det\left[\lambda_i^s(s)I - L^s(s)\right] = 0 \qquad (i = 1,2) \\ &\Rightarrow \quad \lambda_{1,2}(s) = \frac{L_{\alpha\alpha}(s) + L_{\beta\beta}(s)}{2} \pm \sqrt{\left(\frac{L_{\alpha\alpha}(s) - L_{\beta\beta}(s)}{2}\right)^2 + L_{\alpha\beta}(s)L_{\beta\alpha}(s)}. \end{aligned} \tag{25}$$

The non-diagonal terms of the VSC transfer matrix function (11) are usually smaller than the diagonal terms [9], and therefore the non-diagonal terms of the loop transfer function $L^s(s)$ can be neglected in front of the diagonal terms. Considering this approximation, the eigenvalues of the loop transfer function result as

$$\begin{aligned} &\lambda_{1,2}(s) = \frac{L_{\alpha\alpha}(s) + L_{\beta\beta}(s)}{2} \pm \frac{L_{\alpha\alpha}(s) - L_{\beta\beta}(s)}{2} \\ &\Rightarrow \quad \lambda_1(s) = L_{\alpha\alpha}(s) = Y_{vsc\_\alpha\alpha}(s)Z_{g\_\alpha\alpha}(s) \qquad \lambda_2(s) = L_{\beta\beta}(s) = Y_{vsc\_\beta\beta}(s)Z_{g\_\beta\beta}(s). \end{aligned} \tag{26}$$

In this case, the impedance-based and positive-net-damping stability criteria may be directly applied to the αα- and ββ-components for stability assessment. Otherwise, there is not obvious relation between the GNC and the impedance-based- and positive-net-damping stability criteria and further analysis (out of the paper scope) should be made to extend the application of these criteria to MIMO systems. The above comments can also be applied to dq-frame.

B. Study in the s-domain

The positive-net-damping stability criterion of harmonic resonance instabilities can also be demonstrated by analyzing the poles of $F(s)$ or the roots of $1 + L(s) = 0$ in (8). Considering that the dominant pole of the system is the poorly-damped pole related to the harmonic parallel resonance between the grid and the VSC [20] and that around this resonance the VSC has an inductive behavior and the grid has a capacitive behavior (see Section II and example in Section VI), the grid and VSC admittances in (16) can be expressed as follows:

$$Y_g(s) \approx \frac{1}{R_g + 1/(C_g s)} \qquad Y_{vsc}(s) \approx \frac{1}{R_{vsc} + L_{vsc}s}, \tag{27}$$

and the positive-sequence equivalent admittance observed form the VSC current source in Fig. 1(b) is

$$Y_g(j\omega)+Y_{vsc}(j\omega)\approx\frac{1}{R_g-j/(C_g\omega)}+\frac{1}{R_{vsc}+jL_{vsc}\omega}=\frac{R_g+j/(C_g\omega)}{R_g^2+1/(C_g\omega)^2}+\frac{R_{vsc}-jL_{vsc}\omega}{R_{vsc}^2+(L_{vsc}\omega)^2}. \quad (28)$$

The terms R_g^2 and R_{vsc}^2 can be neglected with respect to the terms $1/(C_g\omega)^2$ and $(L_{vsc}\omega)^2$ due to the main capacitive and inductive response of the grid and VSCs. Thus, the equivalent admittance can be approximated as

$$Y_g(j\omega)+Y_{vsc}(j\omega)\approx R_g(C_g\omega)^2+\frac{R_{vsc}}{(L_{vsc}\omega)^2}+j\left(C_g\omega-\frac{1}{L_{vsc}\omega}\right). \quad (29)$$

Moreover, considering (27), $1 + L(s)$ can be written as

$$1+L(s)=1+\frac{R_g+1/(C_g s)}{R_{vsc}+L_{vsc}s}=\frac{C_gL_{vsc}s^2+C_g(R_g+R_{vsc})s+1}{C_g(R_{vsc}+L_{vsc}s)s}. \quad (30)$$

The poles of (30) are

$$s=\frac{-C_g(R_g+R_{vsc})\pm\sqrt{C_g^2(R_g+R_{vsc})^2-4C_gL_{vsc}}}{2C_gL_{vsc}}, \quad (31)$$

which, considering that $C_g(R_g + R_{vsc})^2 << 4L_{vsc}$, can be approximated as

$$s\approx-\frac{R_g+R_{vsc}}{2L_{vsc}}\pm j\frac{1}{\sqrt{C_gL_{vsc}}}. \quad (32)$$

It can be observed that the parallel resonance condition in (29) matches with the imaginary part of the poles in (32). Moreover, according to (29), if (18) holds (i.e., if (29) is passive) at the resonance frequency, the poles have a negative real part:

TABLE II. CHARACTERISTICS OF METHODS FOR STABILITY ASSESSMENT

		State space analysis	Nyquist criterion	Passivity method	Impedance-based criterion	P-n-D criterion	New approach
System data	Detailed	✓	✓	✓	✓	✓	✓
	Measurements	✗	✓	✓	✓	✓	✓
Method evaluation	Simple to evaluate	✗	✓	✓	✓	✓	✓
	Short computation effort	✗	✓	✓	✓	✓	✓
	Consider stability contribution of subsystems	✓	✗	✗	✓	✓	✓
	Provide oscillatory modes	✓	✓	✗	✓	✗	✓
	Provide criterion based on system resistances	✗	✗	✓	✗	✓	✓
Stability analysis	Understand causes of instability	✓	✓	✓	✓	✓	✓
	Interpret physically instabilities	✓	✗	✗	✗	✗	✓

$$G_g(\omega)+G_{vsc}(\omega)=\frac{R_g+R_{vsc}}{(L_{vsc}\omega)^2}>0 \quad \Rightarrow \quad -\frac{R_g+R_{vsc}}{2L_{vsc}}<0. \tag{33}$$

From this demonstration, it can be stated that the frequency at the parallel resonance observed from the VSC current source approximately matches with the frequency of the oscillations in case of instability. Thus, the alternative approach of the positive-net-damping stability criterion based on the phase margin condition allows predicting the frequency of the closed-loop unstable oscillatory modes. It can be observed in (32) that a negative VSC resistance R_{vsc} may lead to a positive real part of the poles if $|R_{vsc}| > |R_g|$ (i.e., to a system instability) which is correctly predicted with the negative value of the net damping $G_g(\omega) + G_{vsc}(\omega)$ in (33).

V. Comparison of Stability Methods

Fig. 3 shows the flowchart of the different methods for stability assessment of grid-connected VSC systems and Table II presents their main characteristics. The state space eigenvalue analysis (or closed-loop root study) is a useful tool to analyze the impact of system and control parameters on stability [8]. However, this method requires detailed information for all elements in the system (including physical and control parameters) and high-order dynamic models for large systems that could exceed the computation limits of the solvers due to the large amount of information to manage from these models which must be update every time if any of the system parameter changes. Moreover, this information is not always completely available limiting an adequate system modeling. On the other hand, frequency domain methods are used to identify the causes of instabilities with less

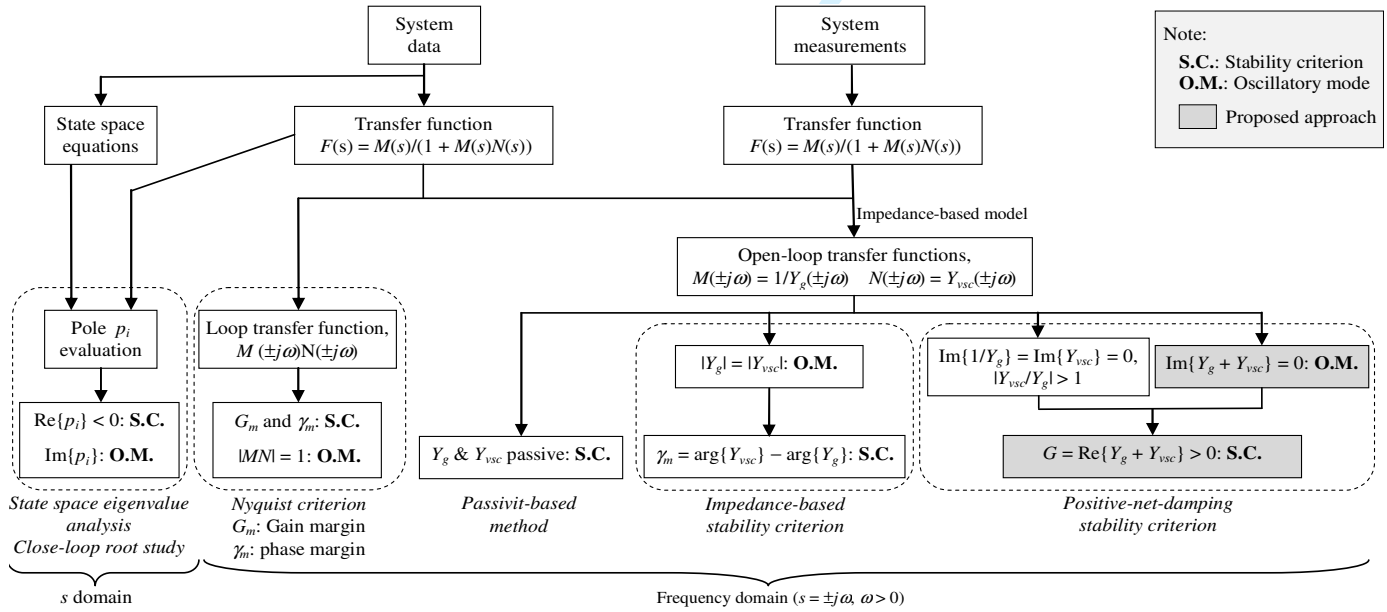

Fig. 3. Flowcharts of stability methods in grid-connected VSC systems.

compute-intensive effort and less detailed system information [9] – [20]. These methods can be applied by using either simulations or system measurements if the system parameter information of analytical models is not available, which offers an advantage over the state space eigenvalue analysis.

The Nyquist criterion and the Bode diagram are the most used frequency domain methods but these methods only show numerical results and they focus on the loop transfer function of the entire system which does not allow investigating separately the contribution of the source and load subsystems to the closed-loop stability [9] – [13]. This may limit the analysis of oscillations and instabilities caused by particular impedances or filters connected to the system even though the loop transfer function could be measured. These drawbacks are avoided with the frequency domain methods that analyze the individual contribution of the source and load subsystems from the open-loop transfer functions [4], [9] – [20]. Among these methods, the passivity-based method imposes passivity in each subsystem (i.e., $G_g(\omega) > 0$ and $G_{vsc}(\omega) > 0$, (16)) for ensuring the closed-loop system stability [4], [13], [14], while the impedance-based and the positive-net-damping stability criteria are less restrictive and do not impose this passivity condition because consider the contribution of each subsystem to stability assessment. As an example, the positive-net-damping stability criterion ensures the closed-loop system stability if $G_g(\omega) + G_{vsc}(\omega) > 0$ (24), and therefore a system could be stable even when VSCs are not passive (i.e., even with $G_{vsc}(\omega) < 0$) if apply $G_g(\omega) > 0$ and $|G_g(\omega)| > |G_{vsc}(\omega)|$. For all the previous comments, the impedance-based criterion [10] – [12] and the positive-net damping criterion based on the gain [19], [20] or phase margin conditions are useful tools for stability analysis offering several advantages in front of the other methods. Based on Fig. 3 and Table II, a comparison between the impedance-based and the positive-net-damping stability criteria is presented below.

According to (18), (19) and (20) and considering that the grid-connected VSC system resistances are smaller than the reactances, the impedance-based method condition $|Y_g(j\omega)| = |Y_{vsc}(j\omega)|$ (i.e., the intersection of the grid and VSC admittances) is equivalent to the condition of the proposed positive-net-damping stability criterion $\mathrm{Im}\{Y_g(j\omega) + Y_{vsc}(j\omega)\} = 0$ (i.e., the parallel resonances between the grid and VSC impedances) and both conditions provide the frequency of the oscillatory modes (see Subsection IV.B). Subsequently, the phase angle between the VSC and the grid admittance ratio (i.e., the phase margin of the loop transfer function, $\gamma_m = \arg\{Y_{vsc}(j\omega)\} - \arg\{Y_g(j\omega)\}$) in the impedance-based method and the net damping $G(\omega) = G_g(\omega) + G_{vsc}(\omega)$ (24) in the proposed positive-net-damping stability criterion are evaluated at the above frequency to analyze stability. The evaluation of the damping stability condition $G_g(\omega) + G_{vsc}(\omega) > 0$ is more practical than the evaluation of the phase margin condition $\gamma_m = \arg\{Y_{vsc}(j\omega)\} - \arg\{Y_g(j\omega)\}$ because damping is directly related to system resistances which are a common parameter in electric power systems (negative or small values of system resistances at specific frequencies may lead to instability problems). Moreover, the damping can be analytically characterized with simpler expressions than the phase margin

because it is easiest handle mathematically the real part of the source and load impedance sum than the phase angle of the source and load impedance ratio. As an example, let assume that the grid is modeled as a capacitor C_g in parallel with the short-circuit resistance R_g and inductance L_g, and the VSC model (6) is determined neglecting the filter resistance (i.e., $R_f = 0$ and $k_i = \alpha_c \cdot R_f = 0$) and considering that $|\omega| >> \{\omega_1, \alpha_f\}$ at the analyzed frequencies [14]. The positive-sequence grid and VSC admittances can be written as

$$\begin{aligned} Y_g(j\omega) &= jC_g\omega + \frac{R_g - jL_g\omega}{R_g^2 + L_g^2\omega^2} \\ Y_{vsc}(j\omega) &\approx \frac{1}{L_f(j\omega + \alpha_c e^{-j\omega T_d})} = \frac{\alpha_c \cos(\omega T_d)}{L_f\left(\omega^2 + \alpha_c^2 - 2\alpha_c\omega\sin(\omega T_d)\right)} + j\frac{\alpha_c \sin(\omega T_d) - \omega}{L_f\left(\omega^2 + \alpha_c^2 - 2\alpha_c\omega\sin(\omega T_d)\right)}, \end{aligned} \tag{34}$$

and the stability conditions of the proposed positive-net-damping stability criteria at the grid and VSC parallel resonances becomes

$$G_g(\omega) + G_{vsc}(\omega) = \frac{R_g}{R_g^2 + L_g^2\omega^2} + \frac{\alpha_c \cos(\omega T_d)}{L_f\left(\omega^2 + \alpha_c^2 - 2\alpha_c\omega\sin(\omega T_d)\right)} > 0, \tag{35}$$

which is much easier to analytically handle and to physically relate with the system resistances that the stability condition of the impedance-based stability criterion because it is analytically complicated to determine the argument of $Y_{vsc}(j\omega)\}$ and $Y_g(j\omega)$. Another example can be found in [22], where the influence of different VSC parameters is graphically analyzed from the VSC damping evaluated with the phase of the VSC transfer function but this study could be performed analytically if the VSC damping had been evaluated with the real part of the VSC transfer function.

The positive-net-damping stability criterion based on the gain margin condition evaluates the net damping at the frequencies derived from the conditions $\mathrm{Im}\{1/Y_g(j\omega)\} \approx 0$, $\mathrm{Im}\{Y_{vsc}(j\omega)\} \approx 0$ and $|Y_{vsc}(j\omega)/Y_g(j\omega)| > 1$ (i.e., at the frequencies of the open-loop resonances and the loop gain greater than 1). Considering (16), these conditions can be expressed as

$$\begin{aligned} &\mathrm{Im}\left\{\frac{1}{Y_g(j\omega)}\right\} \approx 0 \;\Rightarrow\; B_g(\omega) \approx 0 \qquad \mathrm{Im}\{Y_{vsc}(j\omega)\} \approx 0 \;\Rightarrow\; B_{vsc}(\omega) \approx 0 \\ &\left|\frac{Y_{vsc}(j\omega)}{Y_g(j\omega)}\right| = \frac{\sqrt{G_{vsc}^2(\omega) + B_{vsc}^2(\omega)}}{\sqrt{G_g^2(\omega) + B_g^2(\omega)}} > 1 \;\Rightarrow\; G_g^2(\omega) + B_g^2(\omega) > G_{vsc}^2(\omega) + B_{vsc}^2(\omega) \;\Rightarrow\; |B_g(\omega)| \succ |B_{vsc}(\omega)|, \end{aligned} \tag{36}$$

which does match neither with the first gain margin condition (12)

$$\mathrm{Im}\{M(j\omega)N(j\omega)\} = \mathrm{Im}\left\{\frac{G_{vsc}(\omega) + jB_{vsc}(\omega)}{G_g(\omega) + jB_g(\omega)}\right\} = 0 \;\Rightarrow\; G_g(\omega)B_{vsc}(\omega) - G_{vsc}(\omega)B_g(\omega) \approx 0, \tag{37}$$

nor with the first phase margin condition (19), and therefore the frequencies obtained from (36) should not be strictly applied in the second gain and phase margin conditions (13) and (15) to derive the positive-net-damping stability criterion. Moreover, according to (19), the frequency of the oscillatory modes are not characterized by the conditions $|B_g(\omega)| \approx 0$ and $|B_{vsc}(\omega)| \approx 0$ in (36) and it may only be contained in the frequency range defined by $|B_g(\omega)| \succ |B_{vsc}(\omega)|$. This frequency range could be wide depending on the grid-connected VSC system [20]. As alternative, the proposed positive-net-damping stability criterion uses the frequency of the parallel resonances between the grid and VSC impedances. This parallel resonance condition is directly derived from (14), it is easy to determine from the impedance-based characterization of the system and approximately provides the frequencies of the oscillatory modes.

According to the previous comparison, the positive-net-damping stability criterion proposed in the paper offers several advantages respect to the impedance-based and positive-net-damping stability criteria because it collects the best of them, i.e., the evaluation of the net damping, which is more practical than the phase angle between the VSC and the grid admittance ratio, at the parallel resonances between the grid and VSC impedances, which provides specific frequencies related with the oscillatory modes and it is easy to characterize. A recent work in [21] investigates near-synchronous resonance instabilities in grid-connected VSC systems and the impact of PLL on the near-synchronous grid-connected VSC oscillations from the damping at the frequency of the closed-loop oscillatory modes (called as intrinsic oscillatory points). The intrinsic oscillatory points are found from a VSC model which only considers the PI controller. This model leads to a system equivalent impedance with a constant resistance (i.e., the equivalent resistance does not depend on the frequency) and the resonance condition can be directly applied to the imaginary part of the impedance without neglecting the resistance (20). The stability criterion is established from the net damping analysis of the system transfer function at the intrinsic oscillatory points obtained with the simplified VSC

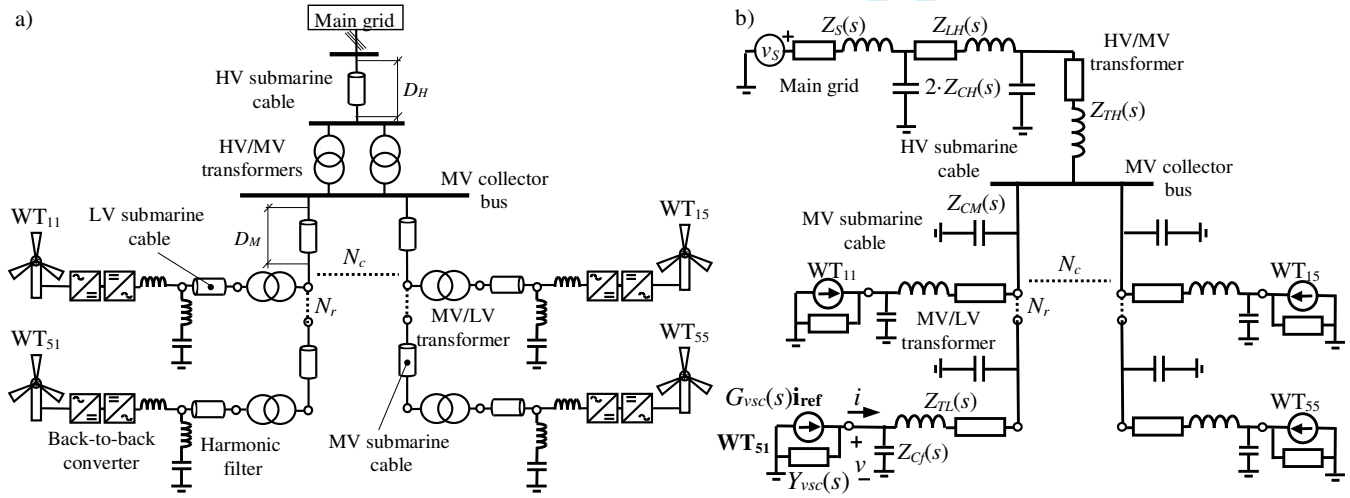

Fig. 4. Offshore WPP system: a) WPP connection scheme. b) Single-line equivalent circuit.

model. This procedure results from the application of the complex torque coefficients method which is presented, but not strictly proof, to study subsynchronous torsional interactions of turbine-generator sets [15], [16]. This method is also used and mathematically analyzed in [17] and [18] presenting some cases where it does not correctly predict closed-loop oscillatory modes and instabilities of the torsional interactions. The proposed approach applies similar as the complex torque coefficients method but it is mathematically demonstrated and extends its application to assess harmonic resonance instabilities in SISO feedback systems and MIMO feedback systems with negligible non-diagonal terms of the loop transfer function (e.g., grid-connected VSC systems). According to the proposed approach, the oscillatory modes are obtained from the parallel resonance between the grid and VSC admittances considering all the system and control parameters of the models. In this case, the resistance of the system equivalent impedance may depend on frequency, and the resonance condition can only be applied if resistances are smaller than reactances.

VI. Application

Application of the different methods to study harmonic resonance instabilities is illustrated in an offshore WPP. The alternative approach of the positive-net-damping stability criterion is compared with the other methods. The application is an example of a grid with multiple VSCs. The connection of multiple VSCs may affect the frequency response of the grid changing the frequency range of its capacitive behavior (i.e., changing the frequency of the parallel resonances) and it may also affect the damping of the grid because the non-passive response of the connected VSCs at the studied frequencies may reduce the grid damping and worsen system stability. However, the above influence does not affect the stability approaches and the assumptions of these approaches as it can be verified in the next Subsections.

Table III. 200 MW Offshore Wind Power Plant Parameters

Main grid	Open-circuit voltage	U_o	150 kV (50 Hz)
	Short-circuit power	S_s	10000MVA
	Ratio X_S/R_S	$\tan\varphi_S$	25
HV/MV transformers	Transformer ratio	$U_{NH}/\ U_{NM}$	150/33 kV
	Rated power	S_N	125 MVA
	Short-circuit impedance	ε_{cc}	0.1 pu
	Ratio X_T/R_T	$\tan\varphi_T$	25
HV submarine cable	Longitudinal π resistance	R_L	0.32 Ω/km
	Longitudinal π reactance	X_L	0.126 Ω/km
	Transversal π reactance	X_C	$0.15{\cdot}10^5$ Ω·km
	Length	D_H	10 km
MV submarine cable	Transversal π reactance	X_C	$0.14{\cdot}10^5$ Ω·km
	Length	D_M	1 km
MV/LV transformer	Transformer ratio	$U_{NM}/\ U_{NL}$	33/0.69 kV
	Rated power	S_N	5 MVA
	Short-circuit impedance	ε_{cc}	0.05 pu
	Ratio X_T/R_T	$\tan\varphi_T$	25
WT	Active power consumption	P_L	5 MW
	Displacement power factor	λ_L	≈ 1.0

A. Description

A 200 MW offshore WPP with 25 type-4 WTs (i.e., full-scale VSC WTs) is studied according to Fig. 4(a). The WPP consists of five 5-WT strings (i.e., $N_r = 5$ and $N_c = 5$). The WTs are connected at 0.69 kV, which is stepped up to 33 kV for the collector system and to 150 kV for the export system with a group of two 125 MVA transformers in parallel. Type-4 WTs are equipped with two converters in back-to-back and harmonic filters are usually installed on the grid side of WT converters to mitigate frequency switching harmonics. Data of the VSC control and the WPP are shown in Table I and Table III, respectively. Instability problems can arise due to the interaction between the grid side VSC control of WTs and the WPP [7]. In order to analyze these problems, the WT VSC and the control are modeled as a Norton equivalent circuit (5) and the offshore WPP is modeled with the equivalent circuit in Fig. 4(b). In the examples, the HV and MV submarine cables are characterized as single concentrated parameter π circuits because they are short enough to be well represented for low frequencies. Moreover, the MV submarine cable model is simplified as the transversal capacitors of the cable because the longitudinal impedance is not significant compared with the inductance of the transformers. On the other hand, the LV submarine cables are omitted because their capacitance is very small and their longitudinal impedance can be included in the impedance of the MV/LV transformer. The Norton equivalent model (5) and the filter capacitance of the WTs are considered in the study.

WPP stability is analyzed from WT_{51} (see Fig. 4(b)). In order to do that, the VSC WT equivalent admittance $Y_{vsc}(s)$ and the offshore WPP equivalent admittance $Y_g(s)$ observed from the analyzed WT must be determined to perform the stability studies. The former is obtained from (6) and the latter is calculated as follows:

$$Y_g(s) = \frac{Z_{Cf}(s) + Z_{TL}(s) + \dfrac{Z_{e1}(s)Z_{CM}(s)}{Z_{e1}(s)+Z_{CM}(s)}}{Z_{Cf}(s)\left(Z_{TL}(s) + \dfrac{Z_{e1}(s)Z_{CM}(s)}{Z_{e1}(s)+Z_{CM}(s)}\right)}, \tag{38}$$

where

$$Z_{e1}(s) = \left((N_r N_c - 1)\left(\frac{1}{Z_{CM}(s)} + \frac{1}{Z_{e2}(s)}\right) + \frac{1}{Z_{e3}(s)}\right)^{-1} \qquad Z_{e2}(s) = \frac{Z_{Cf}(s)/Y_{vsc}(s)}{Z_{Cf}(s) + 1/Y_{vsc}(s)} + Z_{TL}(s)$$
$$Z_{e3}(s) = \frac{Z_{e4}(s)2Z_{CH}(s)}{Z_{e4}(s)+2Z_{CH}(s)} + Z_{TH}(s) \qquad Z_{e4}(s) = \frac{Z_S(s)2Z_{CH}(s)}{Z_S(s)+2Z_{CH}(s)} + Z_{LH}(s). \tag{39}$$

B. Examples

The effect that the VSC control parameters and passive components have on the stability is analyzed. As an example, the influence that the feedforward low-pass filter bandwidth $f_f = \alpha_f/(2\pi)$ (from 1.25 to 2 kHz) and the converter filter inductance L_f (from 0.07 to 0.15 mH) have on WP stability is studied. The WP stability is analyzed from WT_{51} (see Fig. 4(b)) when the

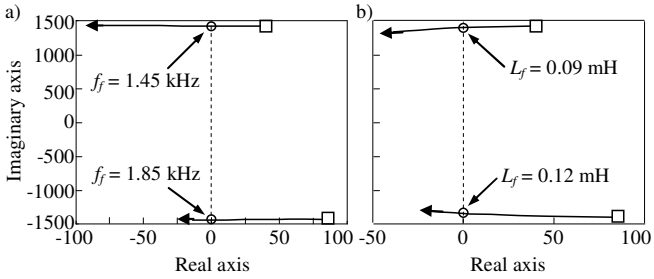

Fig. 5. Root locus of the offshore WPP poles related to the instability: a) Variation of feedforward low-pass filter bandwidth from 1.25 to 2 kHz when L_f = 0.07 mH. b) Variation of converter filter inductance from 0.07 to 0.15 mH when f_f = 1.25 kHz.

parameters $f_f = \alpha_f/(2\pi)$ and L_f of this WT are modified. Note that the VSC feedforward low-pass filter bandwidth is varied from $\alpha_f = 7.85\alpha_c$ to $\alpha_f = 11.9\alpha_c$ considering the low-pass filter design for transient-mode operation in weak grids. The grid and VSC transfer functions are in phase and *dq* coordinates, respectively, and they must be in the same frame to assess stability studies. According to Subsection II.A.2, both transfer functions are transformed to $\alpha\beta$-frame: the VSC transfer function by means of the frequency translation $s \rightarrow s - j\omega_1$ and the grid transfer function is the same as in phase coordinates [23].

The state space eigenvalue analysis (or closed-loop root study) can be used to analyze the impact of system parameters on stability. Multiple poles are numerically obtained from the WPP transfer function and their analysis allows studying the system instabilities. Fig. 5 describes only the root locus of the poles related to instability. These poles are not exactly complex conjugate because the complex gain $jL_f\omega_1$ of the current feedforward in the control law (2) and the transformation of the VSC equivalent admittance from *dq* coordinates to $\alpha\beta$ coordinates by means of the frequency rotation $s \rightarrow s - j\omega_1$ introduce complex components into the closed-loop transfer function $F(s)$ in (8). These components may produce a different frequency response of $F(j\omega)$ and $F(-j\omega)$, $\omega > 0$ since $F^*(j\omega)$ is different from $F(-j\omega)$ (see example in Appendix A) [23]. The system becomes unstable when one of the poles moves to the positive side of the real axis, which is equivalent to a negative damping (see Subsection IV.B). As can be seen from Fig. 5, small values of low-pass filter bandwidth may lead to instability problems whereas large values of converter filter inductances may improve resonance stability. It can also be observed that filter bandwidth does not affect closed-loop oscillatory modes while high filter inductance slightly shifts closed-loop oscillatory modes to lower frequencies.

This application of the frequency-domain methods is shown in Fig. 6 and Fig. 7. Only the frequency response of the positive-sequence ($s = j\omega$, $\omega > 0$) is analyzed because it is the first to cause the system instability (i.e., it is the less damped). A stable and unstable example are illustrated modifying the low-pass filter bandwidth (f_f = 1.9 to 1.25 kHz, respectively) when L_f = 0.07 mH. The Nyquist and Bode diagrams in Fig. 6(a) and Fig. 7(a) confirm the previous results on stability. For f_f = 1.9 kHz, the Nyquist curve does not encircle the −1 point (nor the open-loop system has positive poles) and the Bode plot presents a phase margin equal to ϕ_m = 3.3°. For f_f = 1.25 kHz, the Nyquist curve encircles the −1 point in clockwise direction and the Bode plot presents a

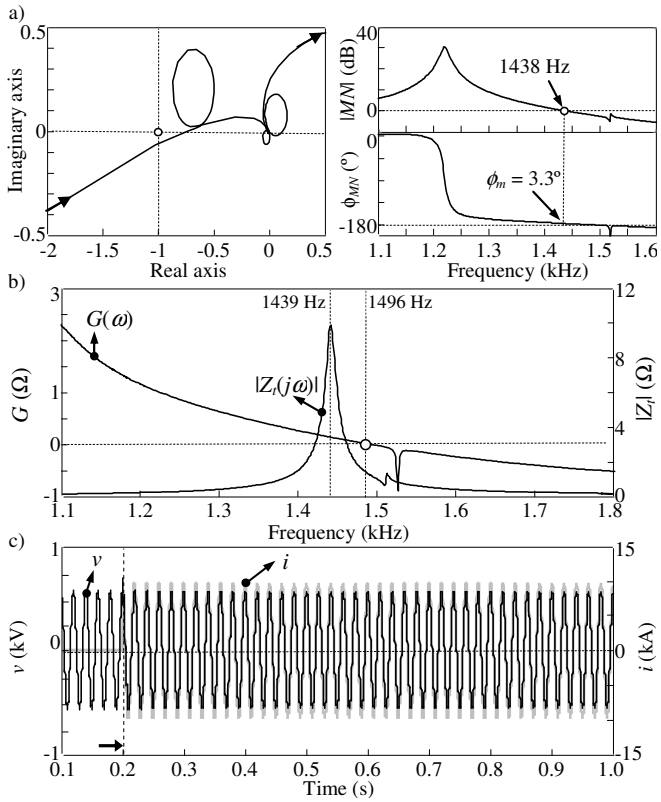

Fig. 6. Stable example of the offshore WPP (L_f = 0.07 mH and f_f = 1.9 kHz): a) Nyquist (left) and Bode (right) plots of $M(j\omega)N(j\omega)$. b) Frequency response of equivalent impedance and damping factor. c) Instantaneous waveforms of the voltage and current at the WT terminals.

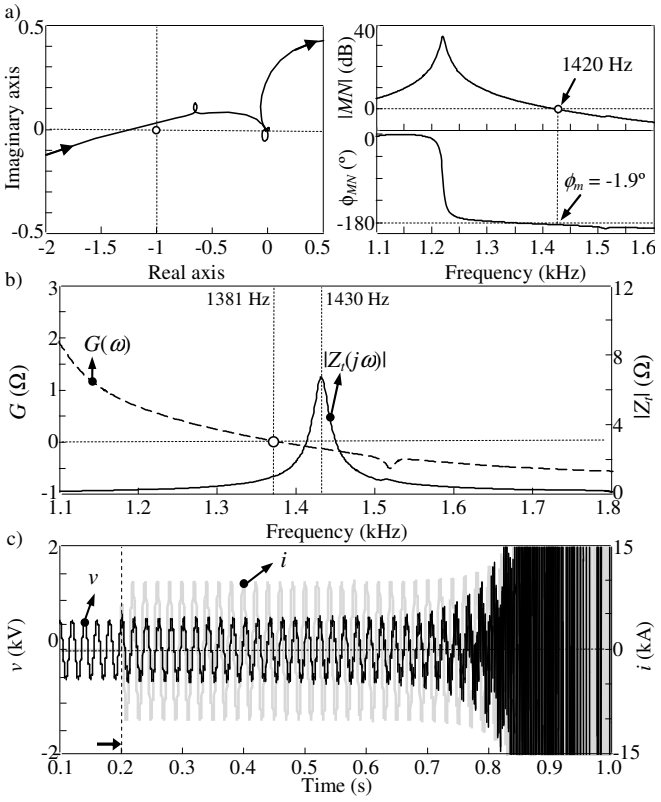

Fig. 7. Unstable example of the offshore WPP (L_f = 0.07 mH and f_f = 1.25 kHz): a) Nyquist (left) and Bode (right) plots of $M(j\omega)N(j\omega)$. b) Frequency response of equivalent impedance and damping factor. c) Instantaneous waveforms of the voltage and current at the WT terminals.

phase margin equal to $\phi_m = -1.9°$. Note that both methods focus on the loop transfer function $L(s) = M(s)\cdot N(s)$ (8) which does not allow investigate separately the contribution of the subsystems $M(s)$ and $N(s)$ to the closed-loop stability.

The application of the alternative approach of the positive-net-damping stability criterion proposed in the paper is shown in Fig. 6(b) and Fig. 7(b). The frequency response of the equivalent impedance $Z_t(j\omega) = (Y_g(j\omega) + Y_{vsc}(j\omega))^{-1}$ (7) and the net damping factor $G(\omega)$ shows that the system is stable for f_f = 1.9 kHz because the $Z_t(j\omega)$ parallel resonance at 1439 Hz is in the positive damping region. The system becomes unstable when f_f = 1.25 kHz due to the negative damping at the $Z_t(j\omega)$ parallel resonance (i.e., at 1430 Hz). These resonances are caused from the interaction between the inductive behavior of the VSC and the capacitive behavior of the grid at these frequencies (see Section II). The cause of the instability is a damping reduction in the VSC contribution because the boundary frequency of the negative damping region is decreased from 1496 Hz to 1381 Hz due to the low-pass filter bandwidth decrease [22]. According to the demonstration in Subsection IV.B, the frequency of the resonance matches with the closed-loop oscillatory modes of the poles in Fig. 5. Note that the alternative approach of the positive-net-damping stability criterion combines the advantages of the eigenvalue analysis and Nyquist and Bode criteria: it is simple to evaluate, as the Nyquist and Bode criterion, and provides information about the cause of instability and the frequency of the oscillatory modes, as the eigenvalue analysis. Moreover, it allows considering the stability contribution of each subsystem. Time-domain simulations in PSCAD/EMTDC are shown in Fig. 6(c) and Fig. 7(c) to validate the stability study. The stable

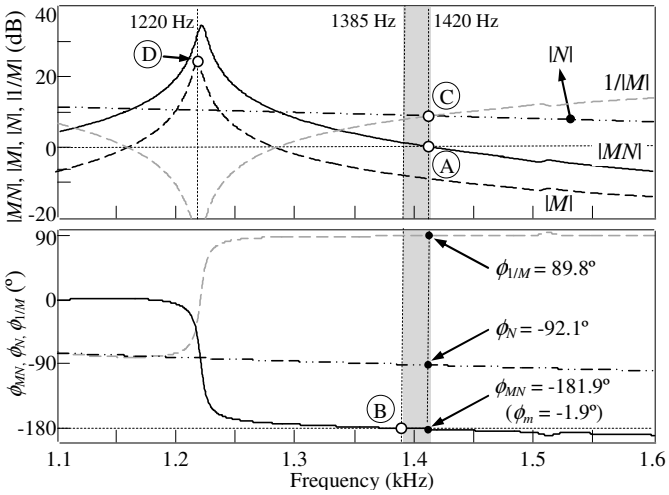

Fig. 8. Comparison of positive-net-damping stability criteria of the offshore WPP unstable example (L_f = 0.07 mH and f_f = 1.25 kHz).

(f_f = 1.9 kHz) and unstable (f_f = 1.25 kHz) waveforms of the instantaneous voltages and currents at the WT_{51} PCC when this WT is connected at 0.2 s are plotted.

C. Comparison with other frequency-domain methods

The alternative approach of the positive-net-damping stability criterion proposed in the paper is further analyzed in Fig. 8, where the unstable situation in Fig. 7 is represented by plotting the Bode diagram of $|N(j\omega)| = |Y_{vsc}(j\omega)|$, $|M(j\omega)| = 1/|Y_g(j\omega)|$, $1/|M(j\omega)|$ and $|M(j\omega)N(j\omega)|$ (9). According to the demonstration in Subsection IV.A.2, the $Z_t(j\omega)$ parallel resonance in Fig. 7 approximately corresponds to the frequency of point A in Fig. 8 where $|M(j\omega)N(j\omega)| = 1$ and the zero crossing point of the net damping factor $G(\omega)$ in Fig. 7 approximately corresponds to point B in Fig. 8 where $\phi_{MN} = -180°$.

The impedance-based stability criterion [10] – [12] analyzes the system stability from the difference between the phases of $Y_{vsc}(j\omega)$ and $Y_{grid}(j\omega)$ at the frequency of point C. This point corresponds to the intersection of the grid and VSC admittance magnitudes $|Y_g(j\omega)|$ and $|Y_{vsc}(j\omega)|$, and the difference between the phases of $Y_g(j\omega)$ and $Y_{vsc}(j\omega)$ characterizes the phase margin of $M(j\omega)N(j\omega)$, i.e., $\phi_m = 180 - (89.8 - 92.1) = -1.9°$ which identifies the system instability. Comparing the proposed positive-net-damping stability criterion with the impedance-based stability criterion, the stability is evaluated at the same frequency for both methods (i.e., the frequency of the parallel resonance of $Z_t(j\omega)$ at point A and the intersection frequency of $|Y_g(j\omega)|$ and $|Y_{vsc}(j\omega)|$ at point C). Also, the evaluation of the net damping factor sign is equivalent to determine phase margin of $M(j\omega)N(j\omega)$ from the difference between the phase of $Y_g(j\omega)$ and $Y_{vsc}(j\omega)$. However, the evaluation of net damping is more practical than the phase evaluation, because the resonance instabilities are related to a lack of damping

The original positive-net-damping stability criterion in [19] analyzes the system stability from the net damping at the open-loop $N(j\omega)$ and $M(j\omega)$ resonances and the frequencies where the loop gain $|M(j\omega)\cdot N(j\omega)|$ exceeds unity. In this case, $N(j\omega)$ does not have any resonance, point D corresponds to the resonance frequency of $M(j\omega)$ and the zone below point A corresponds to the

frequency range where $|M(j\omega)\cdot N(j\omega)|$ exceeds unity. The net damping at point D is positive because the phase of $M(j\omega)\cdot N(j\omega)$ is greater than −180º, and therefore the instability is not predicted by the open-loop transfer function $M(j\omega)$. On the other hand, the net damping at frequencies below point A is negative because the phase between points A and B is smaller than −180º (grey area in Fig. 8) which predicts the system instability. It can be noted that in this example the positive-net-damping stability criterion in [19] assesses the instability of the example from the loop transfer function $M(j\omega)N(j\omega)$ while the proposed positive-net-damping stability criterion assesses this instability from the grid and the VSC admittance contribution at the resonance of the closed-loop system. Comparing the two positive-net-damping stability criteria, both methods are simple to evaluate, but only the proposed positive-net-damping stability criterion always considers the contribution of each subsystem and provides information of the closed-loop oscillatory mode frequencies.

VII. Conclusions

This paper proposes an alternative approach of the positive-net-damping stability criterion for assessing harmonic resonance instabilities. The proposed approach demonstrates mathematically the complex torque coefficients method from the evaluation of the phase margin condition at harmonic resonance frequencies and extends its application to SISO and MIMO feedback systems derived from impedance-based equivalent circuits (e.g., grid-connected VSC systems). This approach can be used if the reactive elements of the system are large compared to the resistive elements (e.g., at the frequencies of the harmonic resonance instabilities in grid-connected VSC systems). The stability criterion proposed in the paper is compared with those in the literature highlighting the following contributions:

- It is simple to evaluate as the frequency domain methods.
- It considers the stability contribution of each subsystem as the impedance-based and positive-net-damping stability criteria.
- It provides an intuitive explanation and physical understanding of the instability phenomenon considering the net damping at electrical resonances as the positive-net-damping criterion.
- It provides a clear relation between harmonic resonances of the grid-connected VSC system and stability.
- It predicts the frequency of the instability oscillations.

Appendix A

Resonance Frequency and System Pole Example

An example is presented to illustrate the different response of the VSC complex transfer function for the positive- and negative-sequences.

Assuming $R_f \approx 0$, $k_i = \alpha_c \cdot R_f \approx 0$, $H(s) \approx 1$ (i.e., the low-filter bandwidth is high to decouple VSC and grid dynamics [2]) and

approximating the VSC time delay T_d by a first-order transfer function [22] as

$$\mathbf{v_o} \approx \frac{1}{T_d s + 1}\mathbf{v_{ref}}, \tag{40}$$

The VSC equivalent admittance (6) can be written in dq-frame as follows,

$$Y_{vsc}(s) = \frac{T_d s}{L_f\left(T_d s^2 + (1 + jT_d\omega_1)s + \alpha_c\right)}, \tag{41}$$

and the poles of the admittance are

$$\begin{aligned} & T_d s^2 + (1 + jT_d\omega_1)s + \alpha_c = 0 \\ \Rightarrow \quad & s_1 = -\frac{1}{2T_d} + \kappa_r + j\left(\kappa_i - \frac{\omega_1}{2}\right) \qquad s_2 = -\frac{1}{2T_d} - \kappa_r - j\left(\kappa_i + \frac{\omega_1}{2}\right), \end{aligned} \tag{42}$$

where

$$\kappa_r + j\kappa_i = \frac{1}{2T_d}\sqrt{(1 + jT_d\omega_1)^2 - 4T_d\alpha_c}. \tag{43}$$

The frequency response of the VSC equivalent impedance for the positive- and negative-sequence is

$$Z_{vsc}(\pm j\omega) = Y_{vsc}^{-1}(\pm j\omega) = \frac{L_f}{T_d} \pm jL_f\left(\omega \pm \omega_1 - \frac{\alpha_c}{T_d\omega}\right), \tag{44}$$

and the resonance frequencies are

$$\mathrm{Im}\{Z_{vsc}(\pm j\omega)\} = 0 \quad \Rightarrow \quad \omega_{\pm} = \sqrt{\left(\frac{\omega_1}{2}\right)^2 + \frac{\alpha_c}{T_d}} \mp \frac{\omega_1}{2}. \tag{45}$$

The poles and the resonance frequency in the $\alpha\beta$-frame become

$$\begin{aligned} & s_1 = -\frac{1}{2T_d} + \kappa_r + j\left(\kappa_i + \frac{\omega_1}{2}\right) \qquad s_2 = -\frac{1}{2T_d} - \kappa_r - j\left(\kappa_i - \frac{\omega_1}{2}\right) \\ & \omega_{\pm} = \pm\frac{\omega_1}{2} + \sqrt{\left(\frac{\omega_1}{2}\right)^2 + \frac{\alpha_c}{T_d}}.. \end{aligned} \tag{46}$$

It can be observed as the system poles are not complex conjugate and the resonance frequency is different for the positive- and negative-sequence due to the feedforward complex gains introduced in the current control loop (e.g., the feedforward term $jL_f\omega_1\mathbf{i}$) and the frequency translations.

APPENDIX B

INDUCTIVE AND CAPACITIVE BEHAVIOR STUDY

Considering that $G_i(\omega) << B_i(\omega)$ for $i = g$ and vsc, (18) can be approximated as $L(j\omega) \approx B_{vsc}(\omega) / B_g(\omega)$. Therefore,

$$\frac{d|L(j\omega)|}{d\omega} \approx \frac{\frac{1}{|B_g(\omega)|}\frac{d|B_{vsc}(\omega)|}{d\omega} - |B_{vsc}(\omega)|\frac{d|B_g(\omega)|}{d\omega}}{|B_g(\omega)|^2}. \tag{47}$$

From (47), the two cases of the second stability condition, (21) and (22), can be identified with the following parallel resonance situations:

- Case #1: Inductive behavior of the grid and capacitive behavior of the VSC, i.e.,

$$\frac{d|B_g(\omega)|}{d\omega} < 0 \quad \text{and} \quad \frac{d|B_{vsc}(\omega)|}{d\omega} > 0 \quad \Rightarrow \quad \frac{d|L(j\omega)|}{d\omega} > 0. \tag{48}$$

- Case #2: Capacitive behavior of the grid and inductive behavior of the VSC, i.e.,

$$\frac{d|B_g(\omega)|}{d\omega} > 0 \quad \text{and} \quad \frac{d|B_{vsc}(\omega)|}{d\omega} < 0 \quad \Rightarrow \quad \frac{d|L(j\omega)|}{d\omega} < 0. \tag{49}$$

REFERENCES

[1] B. Bahrani, *Advanced control strategies for voltage source converters in microgrids and traction networks*, (http://infoscience.epfl.ch/record/181221/files/EPFL_TH5479.pdf), PhD Degree Thesis in Energy, École Polytechnique Féderale de Lausanne, Switzerland, 2011.

[2] A. Yazdani and R. Iravani, *Voltage-sourced converters in power systems. Modeling, control and applications*, John Wiley & Sons, 2010.

[3] L. H. Kocewiak, *Harmonics in large offshore wind farms*, (http://vbn.aau.dk/files/62660098/lukasz_kocewiak.pdf), PhD Degree Thesis in Electrical Engineering, Dep. of Energy Technology, Aalborg University, Denmark, 2012.

[4] L. Harnefors, X. Wang, A. G. Yepes, and F. Blaabjerg, "Passivity-based stability assessment of grid-connected VSCs – An overview," *IEEE Journal and Selected Topics in Power Electronics*, vol. 4, no. 1, pp. 116–125, March 2016.

[5] X. Wang, F. Blaabjerg and W. Wu, "Modeling and analysis of harmonic stability in an AC power electronics-based power systems," *IEEE Transactions on Power Electronics,* vol. 29, no. 12, pp. 6421-6432, Dec. 2014.

[6] E. Möllerstedt and B. Bernhardsson, "Out of control because of harmonics – An analysis of the harmonic response of an inverter locomotive," *IEEE Control Systems Magazine*, vol. 20, no. 4, pp. 70-81, Aug. 2000.

[7] F. D. Freijedo, S. K. Chaudhary, R. Teodorescu, J. M. Guerrero, C. L. Bak, L. H. Kocewiak, and C. F. Jensen, "Harmonic resonances in wind power plants: modeling, analysis and active mitigation methods," *Proc. of the IEEE PowerTech Eindhoven*, June-July 2015, pp. 1-6.

[8] L. P. Kunjumuhammed, B. C. Pal, C. Oates, and K. J. Dyke, "Electrical Oscillations in Wind Farm Systems: Analysis and Insight Based on Detailed Modeling," *IEEE Trans. Sustainable Energy*, vol. 7, no. 1, pp. 51-62, Jan. 2016.

[9] B. Wen, D. Boroyevich, R. Burgos, P. Mattavelli and Z. Shen, "Small-signal stability analysis of three-phase AC systems in the presence of constant power loads based on measurements d-q frame impedances,"*IEEE Transactions on Power Electronics*, vol. 30, no. 10, pp. 5952-5963, Oct. 2015.

[10] J. Sun, "Impedance-based stability criterion for grid-connected inverters," *IEEE Transactions on Power Electronics*, vol. 26, no. 11, pp. 3075–3078, Nov. 2011.

[11] M. Céspedes and J. Sun, "Impedance modelling and analysis of grid-connected voltage-source converters," *IEEE Transactions on Power Electronics*, vol. 29, no. 3, pp. 1254–1261, Nov. 2014.

[12] M. Céspedes and J. Sun, "Impedance shaping of three-phase grid parallel voltage-source converters," 27th Annual IEEE Applied Power Electronics Conference and Exposition (APEC 2012), Feb. 2012, pp. 754–760.

[13] L. Harnefors, L. Zhang, and M. Bongiorno, "Frequency-domain passivity-based current controller design," *IET Power Electronics*, vol. 9, no. 3, p. 1254-1261, 2014.

[14] L. Harnefors, M. Bongiorno and S. Lundberg, "Input-admittance calculation and shaping for controlled voltage-source converters," *IEEE Trans. on Industrial Electronics*, vol. 54, no. 6, pp. 3323-3334, Dec. 2007.

[15] I. M. Canay, "A novel approach to the torsional interaction and electrical damping of the synchronous machine, Part I: Theory," *IEEE Trans. Power App. Syst.*, vol. PAS-101, no. 10, pp. 3630–3638, Oct. 1982.

[16] I. M. Canay, "A novel approach to the torsional interaction and electrical damping of the synchronous machine, Part II: Application to an arbitrary network," *IEEE Trans. Power App. Syst.*, vol. PAS-101, no. 10, pp. 3639–3647, Oct. 1982.

[17] A. Tabesh and R. Iravani, "On the application of the complex torque coefficients method to the analysis of torsional dynamics," *IEEE Trans.Energy Convers.*, vol. 20, no. 2, pp. 268–275, Jun. 2005.

[18] L. Harnefors, "Analysis of subsynchronous torsional interaction with power electronics," *IEEE Trans. on Power Systems*, vol. 22, no. 1, pp. 305-313, Feb. 2007.

[19] L. Harnefors, "Proof and application of the positive-net-damping stability criterion," *IEEE Trans. on Power Systems*, vol. 26, no. 1, pp. 481-482, Feb. 2011.

[20] G. Stamatiou and M. Bongiorno, "Stability Analysis of Two-Terminal VSC-HVDC Systems using Net-Damping Criterion," *IEEE Trans. on Power Delivery*, vol. 31, no. 4, pp. 1748-1756, August 2016.

[21] C. Zhang, M. Molinas and A. Rygg, "Properties and Physical Interpretation of the Dynamic Interactions between Voltage Source Converters and Grid: Electrical Oscillation and Its Stability Control," *IET Power Electronics*, early access, http://dx.doi.org/10.1049/iet-pel.2016.0475.

[22] M. Zhao, X. Yuang, J. Hu. and Y. Yan, "Voltage dynamics of current control time-scale in a VSC-connected weak grid," *IEEE Transactions on Power Systems*, vol. 31, no. 4, pp. 2925-2937, July 2016.

[23] L. Harnefors, "Modeling of Three-Phase Dynamic Systems Using Complex Transfer Functions and Transfer Matrices," *IEEE Transactions on Industrial Electronics,* vol. 54, no. 4, pp. 2239-2248, Aug. 2007.

Response to comments

Title: Positive-Net-Damping Stability Criterion in Grid-Connected VSC Systems

Authors: L.Sainz, M. Cheah-Mane, Ll. Monjo, J. Liang, O. Gomis-Bellmunt

Manuscript ID JESTPE-2017-01-0027

The authors thank the reviewers for their comments and suggestions. Their exhaustive and relevant analysis of the paper has strongly contributed to improve the quality of this work. All modifications resulting from this review have been highlighted in the revised version of the paper using a red font. These modifications are detailed below.

Comments from Editor and Reviewers and Our Responses

Editor's comments:

Comment #1: *As commented by multiple Reviewers, it is claimed in the manuscript that the "VSC behavior is mainly inductive" but no explicit justification of this assumption is presented in the manuscript. Thus, this issue should be further discussed, either by reference to relevant literature or by further elaborations by the authors. It should also be clarified when this assumption is valid, and what limitations this imposes on the application of the method presented in the manuscript.*

The authors agree with the editor's remark. The issue pointed out by the editor is used in several parts of Section IV but it is not explained and justified in detail. There are two assumptions related with the "mainly" inductive and capacitive behavior of the VSC and grid equivalent impedance (or admittance) which are used in the theoretical study of Section IV:

- The first assumption considers that the VSC equivalent impedance behavior is inductive and the grid equivalent impedance behavior is capacitive at the harmonic frequencies.
- The second assumption considers that the resistances (or conductances) of the VSC and grid equivalent impedance (or admittance) can be neglected compared to the inductive or capacitive reactances (or susceptances), and therefore the impedance behavior can be defined as mainly inductive or capacitive.

Regarding the VSC equivalent impedance behavior, there are several studies that illustrate the mainly capacitive or inductive behavior of this impedance depending on the VSC filter elements and the frequency range [R2] – [R6], [12]. Fig. 5 in [R2] illustrates clearly that the equivalent impedance behavior of VSCs with L filter (i.e., the VSC configuration considered in the paper) is mainly capacitive between the fundamental frequency and the current loop crossover frequency while this behavior is

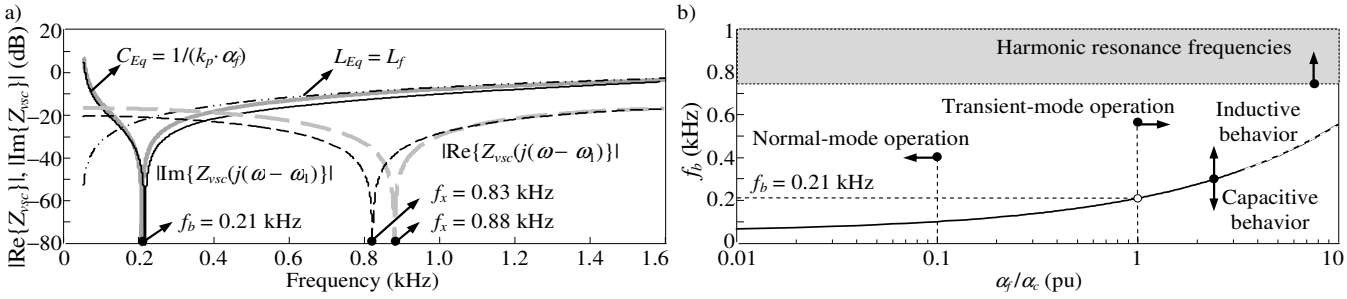

Fig. R1. Study of the VSC equivalent impedance beahavior: a) Real and imaginary parts of $Z_{vsc}(j(\omega - \omega_1)$ [(R1) (in grey) and (6) in black]. b) Boundary frequency versus voltage feedforward low-pass filter bandwidth.

mainly inductive above the current loop crossover frequency. This is supported with experimental measurements in [R2] – [R4], [12]. The frequency range of the capacitive and inductive behavior of VSCs with LC filter is shown in [R5]. An exhaustive analytical study about the influence of the VSC control on the system harmonic response is developed in [R6] providing simplified analytical expressions of the VSC equivalent impedance for harmonic studies. According to [R6], an approximated expression of the positive-sequence VSC equivalent impedance in $\alpha\beta$-frame is presented for $\alpha_f \leq 2.5 \cdot \alpha_c$ and frequencies greater than the grid frequency f_1 (the VSC filter resistance R_f and the integral gain k_i of the PI controller are not considered in the expression),

$$Z_{\text{vsc}}(j(\omega-\omega_1)) \approx (k_p + L_f\alpha_f)\cos\left((\omega-\omega_1)T_d\right) + jL_f\left(\omega-\omega_1-\frac{\alpha_f\alpha_c}{\omega-\omega_1}\right) \qquad (\omega = 2\pi f, \quad \omega_1 = 2\pi f_1), \text{ (R1)}$$

where L_f is the inductance of the VSC filter, $k_p = L_f \cdot \alpha_c$ is the proportional gain of the PI controller, α_c is the closed current control loop bandwidth, α_f is the voltage feedforward low-pass filter bandwidth and T_d is the VSC time delay. Fig. R1(a) compares the frequency response of the VSC equivalent impedance obtained from (R1) and from (6) using the VSC parameter values in Table I (see paper) and $\alpha_f = \alpha_c$ (i.e., $f_f = \alpha_f/(2\pi) = 159$ Hz). It can be observed that the VSC equivalent impedance presents a capacitive and an inductive behavior below and above the boundary frequency f_b. Moreover, it can also be observed that the behavior above the boundary frequency is mainly inductive due to the low contribution of the VSC resistive behavior. At these frequencies, the equivalent impedance approximately matches with the VSC filter reactance. The boundary frequency f_b is obtained by equating to zero the imaginary part of the VSC equivalent impedance (R1)

$$\omega_b - \omega_1 - \frac{\alpha_f\alpha_c}{\omega_b-\omega_1} = 0 \quad \Rightarrow \quad f_b = f_1 + \frac{1}{2\pi}\sqrt{\alpha_f\alpha_c}\,. \qquad \text{(R2)}$$

Fig. R1(b) shows the boundary frequency for the current control loop time constant in Table I (i.e., for $\alpha_c = 1/\tau_c = 1000$ rad/s) and α_f ranging from $0.01 \cdot \alpha_c$ to $10 \cdot \alpha_c$. The frequency range of the harmonic resonance frequencies is also indicated in grey color [R1], [R7]. It is observed that the harmonic resonance frequencies are above the boundary frequency and, according to Fig. R1(a), the behavior of the VSC equivalent impedance at these frequencies is mainly inductive. It is also noted that the lower boundary frequency f_x of the negative damping region can be approximately determined from (R1),

$$\text{Re}\{Z_{\text{vsc}}(j(\omega-\omega_1))\} = (k_p + L_f\alpha_f)\cos\left((\omega-\omega_1)T_d\right) = 0 \quad \Rightarrow \quad f_x = f_1 + \frac{1}{4T_d} \approx \frac{1}{4T_d}. \qquad \text{(R3)}$$

This boundary frequency corresponds to the minimum of $|\text{Re}\{Z_{vsc}(j(\omega-\omega))|$ in Fig. R1(a) and it is close to the harmonic resonance frequencies [14]. Although (R1) does not apply, the above conclusions are also true for the negative-sequence VSC equivalent impedance and for $\alpha_f \geq 2.5 \cdot \alpha_c$.

Regarding the grid equivalent impedance behavior, this impedance may present a capacitive or inductive behavior for different frequency ranges but, according to the above study, the VSC equivalent impedance is mainly inductive at harmonic resonance frequencies, and therefore these resonances are produced by the interaction with the capacitive behavior of the grid equivalent impedance. It is true that other resonances can appear due to the VSC capacitive and grid inductive behavior but these resonances are produced at near-synchronous frequencies which are lower than the boundary frequency f_b. Moreover, the resistive elements of ac grids may be usually neglected compared to the reactive elements and the grid equivalent impedance is commonly characterized by reactances in harmonic resonance studies, i.e. the grid behavior can be considered mainly capacitive at the harmonic resonance frequencies [R2], [R3], [R8], [14].

Considering the above comments, resistances are neglected in the paper to determine the harmonic resonance frequencies (comparison between (19) and (20) and characterize of the imaginary part of the poles in (32)). However, the contribution of these resistances must be considered when the damping of

the system is analyzed (analysis of the second phase margin condition (15) and characterization of the real part of the poles in (32)).

According to the above analysis, the following modifications have been made in the paper:

- The frequency range of the harmonic resonance instabilities analyzed in the paper is indicated in the Introduction to fix the scope of the proposed method:

However, resonance instabilities can appear in poorly damped power systems due to interaction between VSC control and the grid. In general, these resonance instabilities can be classified in two categories [4]: (i) Harmonic resonance instabilities which approximately range from 0.75 to 2 kHz and are caused by negative dampings due to VSC time delay and current control dynamics. (ii) Near-synchronous resonance instabilities which approximately range from 50 to 300 Hz and are caused by negative dampings due to current control dynamics and outer loop controls. The harmonic resonance instabilities are reported in different grid-connected VSC applications such as single-phase ac traction systems [6] and WPPs [7].

- The VSC equivalent impedance behavior is analyzed at the end of Subsection II.A to show the mainly inductive behavior of VSCs at harmonic resonance frequencies.

- The reactive nature of the grid equivalent impedance is commented in the presentation of Fig. 1(b):

The resistive elements of the ac grids may be usually neglected compared to the reactive elements and the impedance $Z_g(s)$ is commonly characterized by reactances in harmonic resonance studies [12], [14], [21].

- The paragraphs below (18) (in Subsection IV.A.2) have been rewritten and the assumption about the mainly reactive (inductive or capacitive) nature of the grid and VSCs at harmonic resonances has been better explained:

Considering the main reactive (inductive or capacitive) nature of the grid and VSCs at harmonic resonances (see Section II), $G_i(\omega) << B_i(\omega)$ for $i = g$, vsc and (18) can be approximated as

$$B_g(\omega) = \pm B_{vsc}(\omega). \tag{19}$$

The parallel resonance observed from the VSC current source in Fig. 1(b), neglecting the conductances $G_g(\omega)$ and $G_{vsc}(\omega)$ with respect to the susceptances $B_g(\omega)$ and $B_{vsc}(\omega)$ due to the main capacitive and inductive nature of the grid and VSCs at the harmonic resonances, can be expressed as

$$\mathrm{Im}\left\{Y_g(j\omega) + Y_{vsc}(j\omega)\right\} \approx 0 \quad \Rightarrow \quad B_g(\omega) \approx -B_{vsc}(\omega), \tag{20}$$

which matches with the negative sign expression in (19).

- The introductory sentence in Subsection IV.B has been reviewed to indicate that the study analyzes the harmonic resonance frequencies and, according to Section II, the VSC has an inductive behavior and the grid has a capacitive behavior at these frequencies:

Considering that the dominant pole of the system is the poorly-damped pole related to the harmonic parallel resonance between the grid and the VSC [20] and that around this resonance the VSC has an inductive behavior and the grid has a capacitive behavior (see Section II and examples in Section VI), the grid and VSC admittances in (16) can be expressed as follows:

- The limitations of the proposed approach are indicated in the demonstration of the positive-net-damping stability criterion (Subsection IV.A.2):

This demonstration can be extended to SISO feedback systems derived from impedance-based equivalent circuits if the equivalent resistances of the circuit are not significant compared to the reactances (i.e., the equivalent impedances of the circuit are mainly inductive or capacitive).

These limitations are also indicated in the Conclusions:

This approach can be used if the reactive elements of the system are large compared to the resistive elements (e.g., at the frequencies of the harmonic resonance instabilities in grid-connected VSC systems).

Comment #2: *In section V.A, the authors are showing a set of root locus plots that is claimed to result from a frequency transformation from the dq coordinates to the alpha-beta coordinates. It is briefly mentioned that this implies that the poles will not be complex conjugate, but that the same stability criteria as for regular eigenvalue analysis apply (i.e. instability in case of minimum one pole with real part higher than 0). However, no further explanation, justification or reference are presented with respect to the background or validity of the applied frequency transformation. Further discussions and explanations supported by appropriate literature is needed to justify the theoretical background for the applied method and the validity of the presented results.*

The following comments describe briefly the applied coordinate transformations and the frequency response studies on transfer functions. The detailed presentation can be found in [R6], [R9], [2].

Three-phase sinuosidal signals x_a, x_b and x_c can be expressed as a complex space vector in stationary coordinates (or $\alpha\beta$-frame) with the coordinate transformation

$$\mathbf{x}^{\mathbf{s}} = x_\alpha + jx_b = \frac{2}{3}\left(x_a + e^{j2\pi/3}x_b + e^{j4\pi/3}x_c\right), \tag{R4}$$

where the complex space vector $\mathbf{x}^{\mathbf{s}}$ in $\alpha\beta$-frame is denoted with bold letters and the superscript s. A symmetrical three-phase system can be characterized in $\alpha\beta$-frame with complex transfer functions $\mathbf{G}^{\mathbf{s}}(s) = G_\alpha(s) + jG_\beta(s)$ which are equal to the complex transfer function in phase coordinates.
The complex space vector $\mathbf{x}^{\mathbf{s}} = \mathrm{x}_\alpha + j\,x_\beta$ in stationary coordinates (or $\alpha\beta$-frame) can be expressed in synchronous coordinates (or dq-frame) with the coordinate transformation

$$\mathbf{x} = x_d + jx_q = e^{-j\theta_1}\mathbf{x}^{\mathbf{s}} \quad \Leftrightarrow \quad \mathbf{x}^{\mathbf{s}} = e^{j\theta_1}\mathbf{x}, \tag{R5}$$

where $d\theta_1/dt = \omega_1$ is the fundamental angular frequency of the three-phase sinusoidal signals. The complex transfer functions in dq-frame $\mathbf{G}(s) = G_d(s) + jG_q(s)$ result from the frequency translation $s \rightarrow s + \mathrm{j}\omega_1$ of the complex transfer function $\mathbf{G}^{\mathbf{s}}(s)$ in $\alpha\beta$-frame, i.e. $\mathbf{G}(s) = \mathbf{G}^{\mathbf{s}}(s + \mathrm{j}\omega_1) \leftrightarrow \mathbf{G}^{\mathbf{s}}(s) = \mathbf{G}(s - \mathrm{j}\omega_1)$.
The transfer function of unsymmetrical systems (e.g., the VSC model considering outer loops) can only be described in $\alpha\beta$- and dq-frame by real space matrices as

$$G^s(s) = \begin{bmatrix} G_{\alpha\alpha}(s) & G_{\alpha\beta}(s) \\ G_{\beta\alpha}(s) & G_{\beta\beta}(s) \end{bmatrix} \quad (u^s = G^s(s)i^s) \qquad G(s) = \begin{bmatrix} G_{dd}(s) & G_{dq}(s) \\ G_{qd}(s) & G_{qq}(s) \end{bmatrix} \quad (u = G(s)i). \tag{R6}$$

where the $\alpha\beta$ and dq complex space vectors are represented by real space vectors (denoted without bold letters) as $x^s = [\mathrm{x}_\alpha, x_\beta]^{\mathrm{T}}$ (i.e. $x^s = [\mathrm{x}_\alpha, x_\beta]^{\mathrm{T}} \leftrightarrow \mathbf{x}^{\mathbf{s}} = \mathrm{x}_\alpha + j\,x_\beta$) and $x = [\mathrm{x}_d, x_q]^{\mathrm{T}}$ (i.e. $x = [\mathrm{x}_d, x_q]^{\mathrm{T}} \leftrightarrow \mathbf{x} = \mathrm{x}_d + j\,x_q$) with $x = u, i$.

Frequency domain methods for stability assessment of closed-loop systems in $\alpha\beta$- or dq-frame must analyze the system response for positive- ($s = j\omega$, $\omega > 0$) and negative- ($s = -j\omega$, $\omega > 0$) sequence space vectors. This study is equivalent to analyze the frequency response for $s = j\omega$, $-\infty < \omega < \infty$. Symmetrical closed-loop systems are modeled by complex transfer functions $F(s) = M(s)/(1 + L(s))$ where

$L(s) = M(s)\cdot N(s)$ is the transfer function of the loop system. In this case, the analysis of the frequency response for $s = \pm j\omega,\ \omega > 0$ (or for $s = j\omega,\ -\infty < \omega < \infty$) is required because the frequency response of $F(j\omega)$ and $F(-j\omega),\ \omega > 0$ may not be equal since $F^*(j\omega)$ may be different from $F(-j\omega)$ [R9]. According to the above comment, the evaluation of the Nyquist curve $L(s)$ for $s = j\omega,\ \omega < 0$ is necessary for applying Nyquist method because this curve may not be the mirror image of the Nyquist curve $L(s)$ for $s = j\omega,\ \omega > 0$ in the real axis [R3], [R9]. Also, the frequency response evaluation of the positive- ($s = j\omega,\ \omega > 0$) and negative- ($s = -j\omega,\ \omega > 0$) sequence complex transfer functions is necessary for applying the impedance-based stability criterion and the positive-net-damping stability criterion because both functions may not be equal [R2], [R3], [11]. This different frequency behavior of the complex transfer functions of symmetrical closed-loop systems is reflected in the poles of the system which may not be complex conjugate. Unsymmetrical closed-loop systems are modeled by real transfer functions as (R6) and the transfer function becomes $F(s) = [\mathrm{I} + L(s)]^{-1}M(s)$ with $L(s) = M(s)\cdot N(s)$. In this case, the stability of the closed-loop system can be analyzed using the generalized Nyquist stability criterion (GNC) for $s = j\omega,\ -\infty < \omega < \infty$ (see response to comment #1 of reviewer #2) where the analysis of the frequency response for $s = j\omega,\ \omega < 0$ (or for $s = -j\omega,\ \omega > 0$) is also required as in the symmetrical case [R5].

Although the editor's remark is an important issue in stability analysis, the authors consider that the paper may not be focused on it because the aim of the work is the proposed approach for stability studies. Nevertheless, they agree with the editor that some explanations are needed to justify the study and results. According to the above comments and the previous presentation of the coordinate transformations and frequency response, the following changes have been made in the paper:

- The frequency transformation of the grid-connected VSC system for stability assessment is clarified at the beginning of Subsection II.A.2:

It must be noted that the grid and VSC transfer functions are in phase and *dq* coordinates, respectively, and they must be in the same frame in Fig. 1(b) to assess stability studies. For that, both transfer functions are expressed in $\alpha\beta$ coordinates with bold letters denoting the space vectors and superscript **s** denoting the $\alpha\beta$-frame (i.e., $\mathbf{x}^{\mathbf{s}} = x_\alpha + j\cdot x_\beta$). The VSC closed-loop transfer function and equivalent admittance in (6) are transformed from *dq* coordinates to $\alpha\beta$ coordinates by means of the frequency translation $s \rightarrow s - \mathrm{j}\omega_1$ and the grid transfer function in phase coordinates is the same as in $\alpha\beta$ coordinates [18], [23].

- The application of the coordinate transformation for analyzing the WPP example in Subsection VI.B has also been clarified:

The grid and VSC transfer functions are in phase and *dq* coordinates, respectively, and they must be in the same frame to assess stability studies. According to Subsection II.A.2, both transfer functions are transformed to $\alpha\beta$-frame: the VSC transfer function by means of the frequency translation $s \rightarrow s - \mathrm{j}\omega_1$ and the grid transfer function is the same as in phase coordinates [23].

- The description of the passivity and stability methods in Section III has been reviewed for pointing out the necessity of their evaluation for the positive- ($s = j\omega,\ \omega > 0$) and negative- ($s = -j\omega,\ \omega > 0$) sequence. The comments have been supported by reference [R9], [11]:

Frequency domain methods for stability assessment must analyze the system response for positive- ($s = j\omega,\ \omega > 0$) and negative- ($s = -j\omega,\ \omega > 0$) sequence because the frequency response of $F(j\omega)$ and $F(-j\omega),\ \omega > 0$ may not be equal since $F^*(j\omega)$ may be different from $F(-j\omega)$ (see example in Appendix A) [11], [23].

- Although the demonstration of the positive-net-damping stability criterion in Subsection IV.A is made for the positive-sequence, it has been commented that the criterion must also be applied for the negative-sequence:

Although these criteria must be evaluated for the positive- ($s = j\omega$, $\omega > 0$) and negative- ($s = -j\omega$, $\omega > 0$) sequence [11], [12], [23], the study below is made considering only the positive sequence for sake of simplicity in the exposition. Nevertheless, the conclusions must also be applied for the negative-sequence.

- A comment about the complex conjugate poles in Subsection VI.B has been included with a sentence supported by the reference [R9]:

These poles are not exactly complex conjugate because the complex gain $jL_f\omega_1$ of the current feedforward in the control law (2) and the transformation of the VSC equivalent admittance from dq coordinates to $\alpha\beta$ coordinates by means of the frequency rotation $s \rightarrow s - j\omega_1$ introduce complex components into the closed-loop transfer function $F(s)$ in (8). These components may produce a different frequency response of $F(j\omega)$ and $F(-j\omega)$, $\omega > 0$ since $F^*(j\omega)$ is different from $F(-j\omega)$ (see example in Appendix A) [23].

An illustrative example has been included in Appendix A (see response to comment #10 of reviewer #3 for more details).

- The stability study in Subsection V.B has only been made for the positive-sequence because it is the first to cause the system instability (note that the pole with positive imaginary part is the first to go into the negative side of the real axis, Fig. 5). This has been mentioned in the presentation of Figs. 6 and 7:

The application of the frequency-domain methods is shown in Fig. 6 and Fig. 7. Only the frequency response of the positive-sequence ($s = j\omega$, $\omega > 0$) is analyzed because it is the first to cause the system instability (i.e., it is the less damped).

If the editor and reviewers consider necessary, the authors are willing to extend the above explanations including more theoretical background about the coordinate transformations and the frequency response studies on transfer functions (e.g., in a new Appendix).

Comment #3: *In general, the literature review and contextualization of the presented approach should be further improved. In general, please consider the first comment of Reviewer 3. However, two particular issues should also be considered by the authors:*

During the review process, some new work has been published, which seems to be based on similar considerations as presented in the manuscript:

C. Zhang et al, "Properties and Physical Interpretation of the Dynamic Interactions between Voltage Source Converters and Grid: Electrical Oscillation and Its Stability Control," in IET Power Electronics, early access, http://dx.doi.org/10.1049/iet-pel.2016.0475

This work also seem consider the resistive part of the VSC impedance, which is neglected without further justification by the authors. Thus, when revising the manuscript, the authors should clarify their contribution also with respect to the most recently available publications.

The authors think that the most important issue in the paper is to clarify the differences between the proposed method and previous work highlighting the contribution of the new approach.

For that, the Introduction has been rewritten to provide only an overview of the stability methods in the literature and Section V has been created for comparing exhaustively these methods. Moreover, a flowchart of the different methods is presented in Fig. 3 and their main caracteristics are summarized in Table II. The recent work in [R8] has also been included in the paper. It is compared with the proposed approach in Section V:

A recent work in [21] investigates near-synchronous resonance instabilities in grid-connected VSC systems and the impact of PLL on the near-synchronous grid-connected VSC oscillations from the damping at the frequency of the closed-loop oscillatory modes (called as intrinsic oscillatory points). The intrinsic oscillatory points are found from a VSC model which only considers the PI controller. This model leads to a system equivalent impedance with a constant resistance (i.e., the equivalent resistance does not depend on the frequency) and the resonance condition can be directly applied to the imaginary part of the impedance without neglecting the resistance (20). The stability criterion is established from the net damping analysis of the system transfer function at the intrinsic oscillatory points obtained with the simplified VSC model. This procedure results from the application of the complex torque coefficients method which is presented, but not strictly proof, to study subsynchronous torsional interactions of turbine-generator sets [15], [16]. This method is also used and mathematically analyzed in [17] and [18] presenting some cases where it does not correctly predict closed-loop oscillatory modes and instabilities of the torsional interactions. The proposed approach applies similar as the complex torque coefficients method but it is mathematically demonstrated and extends its application to assess harmonic resonance instabilities in SISO feedback systems and MIMO feedback systems with negligible non-diagonal terms of the loop transfer function (e.g., grid-connected VSC systems). According to the proposed approach, the oscillatory modes are obtained from the parallel resonance between the grid and VSC admittances considering all the system and control parameters of the models. In this case, the resistance of the system equivalent impedance may depend on frequency, and the resonance condition can only be applied if resistances are smaller than reactances.

The abstract has also been modified including the following paragraph:

The proposed approach allows characterizing the frequency of closed-loop oscillatory modes and identifying the physical and control parameters of the system that increase or reduce the damping of these modes. The extension of the proposed approach to study the stability of Single-Input Single-Output and Multiple-Input Multiple-Output feedback systems is analyzed and the approach is also compared with other stability methods in the literature.

Comment #4:

As an example of analysis, the authors are considering various bandwidths for the low-pass filtering of the voltage feed-forward used in the control of the VSC. Issues related to the impact of the filtering of the voltage feed-forward have been recently discussed in the following publication:

M. Zhao et.al. ,"Voltage Dynamics of Current Control Time-Scale in a VSC-Connected Weak Grid," in IEEE Transactions on Power Systems, vol. 31, no. 4, July 2016, https://doi.org/10.1109/TPWRS.2015.2482605

Thus, the authors should also consider this manuscript as a reference, and comment on the results and approaches of their own results in this context.

The reference commented by the editor, [R10], has been included in the paper because it allows understanding the use of grid voltage feedforward low-pass filters in VSCs and analyzing the impact of the low-pass filter bandwidth on system stability. Several comments based on [R10] ([22] in the paper)

have been written in Section II and Subsection VI.B to clarify the choice of the low-pass filter bandwidth and their influence on stability.

Comments in Section II:

The selection of the low-pass filter bandwidth is a compromise between the stability of the VSC output and the whole system stability [2], [13], [14], [22]. A small vale of this bandwidth is used to keep as narrow as possible the VSC non-passivity region and improve the VSC stability. On the other hand, a large value is required to improve dynamics during fast transients due to grid disturbances which affect stability of VSC terminal voltage. The recommended low-pass filter bandwidth is $\alpha_f \leq 0.1\alpha_c$ for normal-mode operation and $\alpha_f \geq \alpha_c$ for transient-mode operation [14]. If the VSC connects to a stiff bus, the feedforward low-pass filter design $\alpha_f \leq 0.1 \cdot \alpha_c$ ensures steady converter current output [14]. If VSC connects to a weak grid, the feedforward low-pass filter design $\alpha_f \geq \alpha_c$ ensures terminal voltage dynamics stability and avoid that voltage becomes unstable in case of grid disturbances [2], [22].

Comments in Subsection VI.B:

The WP stability is analyzed from WT_{51} (see Fig. 4(b)) when the parameters $f_f = \alpha_f/(2\pi)$ and L_f of this WT are modified. Note that the VSC feedforward low-pass filter bandwidth is varied from $\alpha_f = 7.85\alpha_c$ to $\alpha_f = 11.9\alpha_c$ considering the low-pass filter design for transient-mode operation in weak grids.

…

The cause of the instability is a damping reduction in the VSC contribution because the boundary frequency of the negative damping region is decreased from 1496 Hz to 1381 Hz due to the low-pass filter bandwidth decrease [22].

Reviewer #1 comments:

Comment #1: *Is it really true that the VSC behavior can be considered as mainly inductive? The proportional part of the current controller has the impact of a virtual resistor (at least for lower frequencies where the time delay effect is negligible). Is the behavior really mainly inductive also for a high P gain? Please consider this issue carefully, as several results hinge on the assumption.*

As the reviewer points out, the resistive behavior of the VSC equivalent impedance depends on the proportional gain k_p of the PI controller (R1). However, the VSC behavior at harmonic resonance frequencies for usual values of k_p (e.g., $k_p = \alpha_c L_f$ where α_c is the closed current control loop bandwidth [14]) can be considered mainly inductive as it is shown in Fig. R1 and discussed in the response to the editor's comment #1. This has been clarified when Fig. 2 is commented in Subsection II.A:

It can be observed that for usual values of VSC parameters the VSC equivalent impedance presents a capacitive and an inductive behavior below and above the boundary frequency f_b.

Comment #2: *The bandwidths of the feedforward filter that are considered in Section V seem high. Please elaborate on their selection.*

This issue has been commented in Subsection VI.B and the high value of the feedforward filter bandwidth is justified:

The WP stability is analyzed from WT_{51} (see Fig. 4(b)) when the parameters $f_f = \alpha_f/(2\pi)$ and L_f of this WT are modified. Note that the VSC feedforward low-pass filter bandwidth is varied from $\alpha_f = 7.85\alpha_c$ to $\alpha_f = 11.9\alpha_c$ considering the low-pass filter design for transient-mode operation in weak grids.

Moreover, the presentation of the feedforward low-pass filter bandwidth has been rewritten in Section II to justify better the data in the application (see response to the editor's comment #4). The obtained results when the bandwidth is reduced have been also justified from [R10] in Subsection VI.B:

The WP stability is analyzed from WT_{51} (see Fig. 4(b)) when the parameters $f_f = \alpha_f/(2\pi)$ and L_f of this WT are modified. Note that the VSC feedforward low-pass filter bandwidth is varied from $\alpha_f = 7.85\alpha_c$ to $\alpha_f = 11.9\alpha_c$ considering the low-pass filter design for transient-mode operation in weak grids.

Comment #3: *It seems that the method considers only the current control loop, whereas impact of the outer loops is disregarded. Please elaborate on this; what assumptions are made and how can the outer loops be taken into account?*

The reason of neglecting the outer loops and the consequences of including them into de model are pointed out when Fig. 1(a) is presented at the beginning of Section II:

It must be noted that the converter model in this Section only represents the inner current control loop because the outers loops (e.g., the phase-locked loop, PLL, and the direct-voltage controller, DVC) do not affect harmonic resonance instabilities in the 0.75 kHz to 2 kHz frequency range due to their low bandwidths [4], [5]. It can be observed that the transfer matrices of the VSC models in [14] become the common diagonal matrices of the VSC inner current control loop for frequencies greater than the low bandwidths of the outer control loops. This assumption allows a VSC symmetrical model to be obtained which can be characterized with complex impedances or admittances. If outer loops are included, the system becomes nonlinear and VSCs must be represented by real vectors and transfer matrices leading to a two-dimensional MIMO model [23].

The procedure to address MIMO system stability from the positive-net-damping stability criterion is commented at the end of Subsection II.B and Subsection IV.A (see also response to comment #1 of reviewer #2).

Comment #4: *Explain in detail how your work differs from the related [17]*

The authors hope that Section V with Fig. 3 and Table II clarifies the reviewer concern. A comparison between the positive-net-damping stability criterion based on the gain margin condition and the positive-net-damping stability criterion proposed in the paper is included in this Section:

The positive-net-damping stability criterion based on the gain margin condition evaluates the net damping at the frequencies derived from the conditions $\mathrm{Im}\{1/Y_g(j\omega)\} \approx 0$, $\mathrm{Im}\{Y_{vsc}(j\omega)\} \approx 0$ and $|Y_{vsc}(j\omega)/Y_g(j\omega)| > 1$ (i.e., at the frequencies of the open-loop resonances and the loop gain greater than 1). Considering (16), these conditions can be expressed as

$$\mathrm{Im}\left\{\frac{1}{Y_g(j\omega)}\right\}\approx 0 \;\Rightarrow\; B_g(\omega)\approx 0 \qquad \mathrm{Im}\{Y_{vsc}(j\omega)\}\approx 0 \;\Rightarrow\; B_{vsc}(\omega)\approx 0$$

$$\left|\frac{Y_{vsc}(j\omega)}{Y_g(j\omega)}\right| = \frac{\sqrt{G_{vsc}^2(\omega)+B_{vsc}^2(\omega)}}{\sqrt{G_g^2(\omega)+B_g^2(\omega)}} > 1 \;\Rightarrow\; G_g^2(\omega)+B_g^2(\omega) > G_{vsc}^2(\omega)+B_{vsc}^2(\omega) \tag{36}$$

$$\Rightarrow \;\left|B_g(\omega)\right| \succ \left|B_{vsc}(\omega)\right|,$$

which does match neither with the first gain margin condition (12)

$$\mathrm{Im}\{M(j\omega)N(j\omega)\} = \mathrm{Im}\left\{\frac{G_{vsc}(\omega)+jB_{vsc}(\omega)}{G_g(\omega)+jB_g(\omega)}\right\} = 0 \;\Rightarrow\; G_g(\omega)B_{vsc}(\omega)-G_{vsc}(\omega)B_g(\omega)=0, \tag{37}$$

nor with the first phase margin condition (19), and therefore the frequencies obtained from (36) should not be strictly applied in the second gain and phase margin conditions (13) and (15) to derive the positive-net-damping stability criterion. Moreover, according to (19), the frequency of the oscillatory modes are not characterized by the conditions $|B_g(\omega)|\approx 0$ and $|B_{vsc}(\omega)|\approx 0$ in (36) and it may only be contained in the frequency range defined by $|B_g(\omega)| \succ |B_{vsc}(\omega)|$. This frequency range could be wide depending on the grid-connected VSC system [20]. As alternative, the proposed positive-net-damping stability criterion uses the frequency of the parallel resonances between the grid and VSC impedances. This parallel resonance condition is directly derived from (14), it is easy to determine from the impedance-based characterization of the system and approximately provides the frequencies of the oscillatory modes.

Reviewer #2 comments:

Comment #1: *The method and results are presented for SISO system. However, the grid tied VSCs are MIMO system in terms of the impedance since the impedances are positive-negative sequence impedance in sequence domain [1] and dq-impedance in dq-frame [2]. When the impedance based analysis is carried out by checking the Nyquist criterion, the stability analysis is performed for MIMO Nyquist criteria. How this issue can be addressed in the positive net damping stability method.*

The MIMO systems are introduced at the end of Subsection II.B:

If the outer loops are considered in the VSC characterization, the VSC model in $\alpha\beta$- or dq-frame is a two-dimensional MIMO system because VSC must be represented by real vectors and transfer matrices. The impedance-based representation of the grid-connected VSC system (8) becomes [23],

$$F^s(s) = \left[I + L^s(s)\right]^{-1} Z_g^s(s) \qquad L^s(s) = Y_{vsc}^s(s) Z_g^s(s), \tag{10}$$

where, considering $\alpha\beta$-frame,

$$Y_{vsc}^s(s) = \begin{bmatrix} Y_{vsc\_\alpha\alpha}(s) & Y_{vsc\_\alpha\beta}(s) \\ Y_{vsc\_\beta\alpha}(s) & Y_{vsc\_\beta\beta}(s) \end{bmatrix} \qquad Z_g^s(s) = \begin{bmatrix} Z_{g\_\alpha\alpha}(s) & 0 \\ 0 & Z_{g\_\beta\beta}(s) \end{bmatrix}$$

$$L^s(s) = \begin{bmatrix} L_{\alpha\alpha}(s) & L_{\alpha\beta}(s) \\ L_{\beta\alpha}(s) & L_{\beta\beta}(s) \end{bmatrix} = \begin{bmatrix} Y_{vsc\_\alpha\alpha}(s)Z_{g\_\alpha\alpha}(s) & Y_{vsc\_\alpha\beta}(s)Z_{g\_\beta\beta}(s) \\ Y_{vsc\_\beta\alpha}(s)Z_{g\_\alpha\alpha}(s) & Y_{vsc\_\beta\beta}(s)Z_{g\_\beta\beta}(s) \end{bmatrix}. \tag{11}$$

The procedure to address the MIMO system stability from the positive-net-damping stability criterion is commented at the end of Subsection IV.A.2:

If the outer loops are considered in the VSC characterization, the VSC model in *αβ*- or *dq*-frame is a two-dimensional MIMO system (10) and the stability must be analyzed using the generalized Nyquist stability method (GNC) which extends the traditional Nyquist criterion to the eigenloci of the system return-ratio matrix (i.e., to the Nyquist curves of the eigenvalues of the loop gain transfer matrix) [9], [23]. These eigenvalues are obtained from the loop transfer function $L^s(s)$ (11),

$$\det\left[\lambda_i^s(s)I - L^s(s)\right] = 0 \qquad (i = 1,2)$$
$$\Rightarrow \quad \lambda_{1,2}(s) = \frac{L_{\alpha\alpha}(s) + L_{\beta\beta}(s)}{2} \pm \sqrt{\left(\frac{L_{\alpha\alpha}(s) - L_{\beta\beta}(s)}{2}\right)^2 + L_{\alpha\beta}(s)L_{\beta\alpha}(s)}. \tag{25}$$

The non-diagonal terms of the VSC transfer matrix function (11) are usually smaller than the diagonal terms [9], and therefore the non-diagonal terms of the loop transfer function $L^s(s)$ can be neglected in front of the diagonal terms. Considering this approximation, the eigenvalues of the loop transfer function result as

$$\lambda_{1,2}(s) = \frac{L_{\alpha\alpha}(s) + L_{\beta\beta}(s)}{2} \pm \frac{L_{\alpha\alpha}(s) - L_{\beta\beta}(s)}{2}$$
$$\Rightarrow \quad \lambda_1(s) = L_{\alpha\alpha}(s) = Y_{vsc\_\alpha\alpha}(s)Z_{g\_\alpha\alpha}(s) \qquad \lambda_2(s) = L_{\beta\beta}(s) = Y_{vsc\_\beta\beta}(s)Z_{g\_\beta\beta}(s). \tag{26}$$

In this case, the impedance-based and positive-net-damping stability criteria may be directly applied to the αα- and ββ-components for stability assessment. Otherwise, there is not obvious relation between the GNC and the impedance-based- and positive-net-damping stability criteria and further analysis (out of the paper scope) should be made to extend the application of these criteria. The above comments can also be applied to *dq*-frame.

Comment #2: *PLL is used to synchronize VSC with the grid frequency. The control system shown in fig. 1 (a) is based on dq-frame control which should have a PLL.*

The reviewer is true but the outer control loops as the phase-locked loop (PLL) are not considered in the study. The reason of the outer control loops disregarding (e.g., the PLL) is pointed out when Fig. 1(a) is presented at the beginning of Section II:

It must be noted that the converter model in this Section only represents the inner current control loop because the outers loops (e.g., the phase-locked loop, PLL, and the direct-voltage controller, DVC) do not affect harmonic resonance instabilities in the 0.75 kHz to 2 kHz frequency range due to their low bandwidths [4], [5].

Comment #3: *In Section IV.B authors assumed that the grid impedance is capacitive. This assumption is not true for all the cases. The authors should clearly identify when the assumption is valid. Similar, the VSC impedance is assumed to be inductive and is represented by a simple RL circuit in the analysis. The reviewer believes, this assumption is not also true. Authors can have a look on the impedance analysis of grid tied VSC [1,2].*

[1] M. Cespedes and J. Sun, "Impedance Modeling and Analysis of Grid-Connected Voltage-Source Converters," in IEEE Transactions on Power Electronics, vol. 29, no. 3, pp. 1254-1261, March 2014
[2]B. Wen, D. Boroyevich, R. Burgos, P. Mattavelli and Z. Shen, "Analysis of D-Q Small-Signal Impedance of Grid-Tied Inverters," in IEEE Transactions on Power Electronics, vol. 31, no. 1, pp. 675-687, Jan. 2016

It is true that the VSC and grid equivalent impedances can be capacitive or inductive depending on frequency but the VSC equivalent impedance behavior at harmonic resonance frequencies is mainly inductive, and therefore the harmonic resonance is produced by a capacitive grid equivalent impedance (see response to editor's comment #1). For this reason, the VSC inductive and grid capacitive behavior is assumed in the study of the system poles in Subsection IV.B.

Comment #4: *The theoretical analysis is based on the ratio of the grid and VSC impedance. In figs. 4(b) and 5 (b), the stability analysis has been carried out based on the total impedance. The total impedance has not been defined in the paper which makes the reviewer confused in understanding the analysis*

The impedance $Z_t(j\omega)$ has been defined in (7). It is the parallel equivalent impedance of the grid and VSC impedances which allows identifying the frequency of the harmonic parallel resonance between the grid and VSC impedances (see demonstration in response to comment #1.c of reviewer #4). This has been indicated below (20):

The parallel resonance can also be obtained from the parallel equivalent impedance $Z_t(j\omega)$ (7).

Reviewer #3 comments:

Comment #1: *The most important comment to the paper is to write more clear how the proposed method distinguishes from previous work. Both the abstracts and introduction give some hints, but do not write explicitly what is the core contribution of the paper. The information gathered from by the proposed method seems to be identical to the information obtained with a Nyquist plot, apart from another kind of stability margin (damping vs. phase or gain margin). If this is the case, the author should put more emphasis on explaining why the damping is a better measure of stability margin*

Fig. 3 and Table II in Section V have been included to clarify the reviewer concern. A comparison between the Nyquist criterion and the other methods is included in this Section:

The Nyquist criterion and the Bode diagram are the most used frequency domain methods but these methods only show numerical results and they focus on the loop transfer function of the entire system which does not allow investigating separately the contribution of the source and load subsystems to the closed-loop stability [9] – [13]. This may limit the analysis of oscillations and instabilities caused by particular impedances or filters connected to the system even though the loop transfer function could be measured. These drawbacks are avoided with the frequency domain methods that analyze the individual contribution of the source and load subsystems from the open-loop transfer functions [4], [9] – [20].

Comment #2: *Based on the above comment it is suggested to provide a description of the proposed method either in list or flowchart format. Then the reader does not have the read the paper in detail to understand the contribution*

The authors agree with the reviewer suggestion. Fig. 3 and Table II in Section V have been included to compare the different methods and understand the contribution of the proposed approach.

Comment #3: *Page 1: "A good method should not require detailed knowledge of the system". Then it is argued that the frequency-domain methods do not require detailed information. This is true as long as the impedance is obtained by simulation or measurements, but most publications, including the paper under review, is based on analytical models. Then, detailed system information is in fact needed. The authors should rephrase the introduction based on this discussion, or argue better if they disagree.*

A comparison between the state-space eigenvalue analysis and the frequency domain methods is included in Section V:

The state space eigenvalue analysis (or closed-loop root study) is a useful tool to analyze the impact of system and control parameters on stability [8]. However, this method requires detailed information for all elements in the system (including physical and control parameters) and high-order dynamic models for large systems that could exceed the computation limits of the solvers due to the large amount of information to manage from these models which must be update every time if any of the system parameter changes. Moreover, this information is not always completely available limiting an adequate system modeling. On the other hand, frequency domain methods are used to identify the causes of instabilities with less compute-intensive effort and less detailed system information [9] – [20]. These methods can be applied by using either simulations or system measurements if the system parameter information of analytical models is not available, which offers an advantage over the state space eigenvalue analysis.

As the reviewer comment, most publications use frequency domain methods from analytical models. However, there are also some publications that assess stability problem by means of system measurements highlighting the advantages of these methods with respect to state space eigenvalue analysis [R2] – [R5], [11]. The authors think that the works based on analytical models are most common because researchers cannot easily access measurements.

Comment #4: *There seems to be an error in (11). Right hand side is a complex number, which cannot be compared to "-1". Perhaps the author meant to take the absolute value of the left-hand side, i.e. requiring that the minor loop gain is outside the unit circle?*

Note that the paragraph above (12) and (13) comments that both conditions must be verify at the same frequency. Therefore, $M(j\omega)N(j\omega)$ is a real number at the frequency of the condition $\mathrm{Im}\{M(j\omega)N(j\omega)\} = 0$. In particular, the $M(j\omega)N(j\omega)$ value at this frequency is the cross point of the Nyquist curve $L(s)$ with the real axis A short sentence has been written below (13) to explain better the meaning of (12) and (13):

Note that the $M(j\omega)N(j\omega)$ value at the frequency of (12) is the cross point of the Nyquist curve $L(s)$ with the real axis which should be on the right hand side of −1 for stability assessment, i.e. (13) may be hold.

Comment #5: *Page 12: The equivalent impedance Zt(jw) is not defined in the paper as far as the reviewer can tell (maybe he is mistaken). It is important to define this impedance since it is used to explain the proposed method. The reviewer expects this impedance to be the sum of grid and converter impedance, but he is not sure*

The impedance $Z_t(j\omega)$ has been defined in (7). It is the parallel equivalent impedance of the grid and VSC impedances which allows identifying the frequency of the harmonic parallel resonance between the grid and the VSC impedances (see demonstration in response to comment #1.c of reviewer #4). This has been indicated below (20).

Comment #6: *In some equations (e.g. (18)), the sum of converter and grid admittance is used to analyze stability, while in Fig. 4 and 5 it seems that the sum of impedance is used to analyze stability. Which sum should be applied when using the proposed method: impedance, admittance or both? Will both sums give the same result?*

The authors hope that the response to comment #5 answers this reviewer remark.

Comment #7: *Why is the legend in Fig 5b including both Zt and Zg when there is only one impedance curve? Similarly, both G and Gvsc when there is only one damping factor curve*

The mistake has been corrected.

Comment #8: *The sentence "However, the evaluation of net damping is more practical than the phase evaluation, because the resonance instabilities are related to a lack of damping" and similar sentences are used several places in the paper. It is used to argue that the proposed method is more convenient than the impedance-based stability criterion. Can the authors elaborate better what they mean by "practical" in this respect? It is not made clear for the reviewer that the proposed method is advantageous compared with the impedance-based stability criterion. In his opinion, the phase margin is also a clear and intuitive measure of stability margin.*

It is true that phase margin is as clear and intuitive as damping to evaluate system stability. Authors refer to other idea with the term "practical" but they did not present correctly this idea. This issue has been clarified in Section V:

The evaluation of the damping stability condition $G_g(\omega) + G_{vsc}(\omega) > 0$ is more practical than the evaluation of the phase margin condition $\gamma_m = \arg\{Y_{vsc}(j\omega)\} - \arg\{Y_g(j\omega)\}$ because damping is directly related to system resistances which are a common parameter in electric power systems (negative or small values of system resistances at specific frequencies may lead to instability problems). Moreover, the damping can be analytically characterized with simpler expressions than the phase margin because it is easiest handle mathematically the real part of the source and load impedance sum than the phase angle of the source and load impedance ratio. As an example, let assume that the grid is modeled as a capacitor C_g in parallel with the short-circuit resistance R_g and inductance L_g, and the VSC model (6) is determined neglecting the filter resistance (i.e., $R_f = 0$ and $k_i = \alpha_c \cdot R_f = 0$) and considering that $|\omega| >> \{\omega_1, \alpha_f\}$ at the analyzed frequencies [14]. The positive-sequence grid and VSC admittances can be written as

$$Y_g(j\omega) = jC_g\omega + \frac{R_g - jL_g\omega}{R_g^2 + L_g^2\omega^2}$$
$$Y_{vsc}(j\omega) \approx \frac{1}{L_f(j\omega + \alpha_c e^{-j\omega T_d})} = \frac{\alpha_c \cos(\omega T_d)}{L_f\left(\omega^2 + \alpha_c^2 - 2\alpha_c\omega\sin(\omega T_d)\right)} + j\frac{\alpha_c \sin(\omega T_d) - \omega}{L_f\left(\omega^2 + \alpha_c^2 - 2\alpha_c\omega\sin(\omega T_d)\right)}, \quad (34)$$

and the stability condition of the proposed positive-net-damping stability criteria at the grid and VSC parallel resonances becomes

$$G_g(\omega) + G_{vsc}(\omega) = \frac{R_g}{R_g^2 + L_g^2\omega^2} + \frac{\alpha_c \cos(\omega T_d)}{L_f\left(\omega^2 + \alpha_c^2 - 2\alpha_c\omega\sin(\omega T_d)\right)} > 0, \quad (35)$$

which is much easier to analytically handle and to physically relate with the system resistances that the stability condition of the impedance-based criterion because it is analytically complicated determined the argument of $Y_{vsc}(j\omega)\}$ and $Y_g(j\omega)$. Other example can be found in [22], where the influence of different VSC parameters is graphically analyzed from the VSC damping evaluated with the phase of the VSC transfer function but this study could be performed analytically if the VSC damping had been evaluated with the real part of the VSC transfer function.

Comment #9: *Equations (27) and (28) are useful, but several assumptions are made in order to derive them. It is suggested to structure this section better, so it will be easier to understand when the equations are valid*

The authors hope that the explanation to editor's comment #1 will contribute to clarify the assumptions in Subsection IV.B. Nevertheless, they are willing to structure this Subsection better if the reviewer considers necessary yet.

Comment #10: *In Fig 3 – a frequency shift is performed in order to obtain the state space model. Does this mean the state space model is in alpha betta coordinates? If the state space model was analyzed in the dq domain, it is expected that the eigenvalues are complex conjugate. The eigenvalues in Fig 3 are not complex conjugate. In the understanding of the reviewer, the system should have the same eigenvalues regardless of modeling domain – can the authors please elaborate on this and/or suggest a reference where state-space modeling is performed in phase domain coordinates?*

The frequency transformation of the grid-connected VSC system for stability assessment is clarified in Subsection II.A.2 and Subsection VI.B (see response to the editor's comment 2).

References [R2] and [11] characterize the impedance-based model of the grid-connected VSCs in phase and *dq*-frame analyzing the differences between them.

The stability study must provide the same conclusions regardless of the frame but the poles of the system may change. According to this, the authors present two illustrative examples:

Example 1:

Consider the equivalent impedance transfer function of a capacitor in parallel with an RL impedance in phase domain and their corresponding poles,

$$u = Z(s)i \qquad Z(s) = \frac{(R+Ls)\frac{1}{Cs}}{R+Ls+\frac{1}{Cs}} = \frac{R+Ls}{CLs^2+RCs+1} \quad \Rightarrow \quad s_{1,2} = -\frac{R}{2L} \pm \sqrt{\frac{R^2}{4L^2} - \frac{1}{LC}}. \tag{R7}$$

If the transfer function is expressed in *dq*-frame by means of the frequency translation $s \rightarrow s + \mathrm{j}\omega_1$, the poles are

$$s_{1,2} = -\frac{R}{2L} - j\omega_1 \pm \sqrt{\frac{R^2}{4L^2} - \frac{1}{LC}}. \tag{R8}$$

It can be observed as the system poles depend on the frame due to the frequency translation. It can also be observed that the poles in *dq*-frame are not complex conjugate. This translation shifts the frequency response of the admittances (or impedances).

Example 2:

Assuming $R_f \approx 0$, $k_i = \alpha_c \cdot R_f \approx 0$, $H(s) \approx 1$ (i.e., the low-filter bandwidth is high to decouple VSC and grid dynamics [2]) and approximating the VSC time delay T_d by a first-order transfer function [R10],

$$\mathbf{v_o} \approx \frac{1}{T_d s + 1} \mathbf{v_{ref}}, \tag{R9}$$

The VSC equivalent admittance (6) can be written in *dq*-frame as follows,

$$Y_{vsc}(s)=\frac{T_d s}{L_f\left(T_d s^2+(1+jT_d\omega_1)s+\alpha_c\right)}, \tag{R10}$$

and the poles of the admittance are

$$\begin{aligned} &T_d s^2+(1+jT_d\omega_1)s+\alpha_c=0 \\ &\Rightarrow \quad s_1=-\frac{1}{2T_d}+\kappa_r+j\left(\kappa_i-\frac{\omega_1}{2}\right) \qquad s_2=-\frac{1}{2T_d}-\kappa_r-j\left(\kappa_i+\frac{\omega_1}{2}\right), \end{aligned} \tag{R11}$$

where

$$\kappa_r+j\kappa_i=\frac{1}{2T_d}\sqrt{(1+jT_d\omega_1)^2-4T_d\alpha_c}. \tag{R12}$$

The frequency response of the VSC equivalent impedance for the positive- and negative-sequence is

$$Z_{vsc}(\pm j\omega)=Y_{vsc}^{-1}(\pm j\omega)=\frac{L_f}{T_d}\pm jL_f\left(\omega\pm\omega_1-\frac{\alpha_c}{T_d\omega}\right), \tag{R13}$$

and the resonance frequencies are

$$\mathrm{Im}\{Z_{vsc}(\pm j\omega)\}=0 \quad \Rightarrow \quad \omega_{\pm}=\sqrt{\left(\frac{\omega_1}{2}\right)^2+\frac{\alpha_c}{T_d}}\mp\frac{\omega_1}{2}. \tag{R14}$$

It can be observed as the system poles (R12) are not complex conjugate and the resonance frequency (R14) is different for the positive- and negative-sequence due to the feedforward term $jL_f\omega_1\mathbf{i}$.
The poles and the resonance frequency in the $\alpha\beta$-frame are

$$\begin{aligned} &s_1=-\frac{1}{2T_d}+\kappa_r+j\left(\kappa_i+\frac{\omega_1}{2}\right) \qquad s_2=-\frac{1}{2T_d}-\kappa_r-j\left(\kappa_i-\frac{\omega_1}{2}\right) \\ &\omega_{\pm}=\pm\frac{\omega_1}{2}+\sqrt{\left(\frac{\omega_1}{2}\right)^2+\frac{\alpha_c}{T_d}}. \end{aligned} \tag{R15}$$

In general, the poles are not complex conjugate due to the frequency translations and the feedforward complex gains introduced in the current control loop (e.g., the feedforward term $jL_f\omega_1\mathbf{i}$). It is also true for the difference between the positive- and negative-sequence resonance frequencies.

A comment about the complex conjugate poles in Subsection VI.B has been included on the basis of the previous analysis:

These poles are not exactly complex conjugate because the complex gain $jL_f\omega_1$ of the current feedforward in the control law (2) and the transformation of the VSC equivalent admittance from dq coordinates to $\alpha\beta$ coordinates by means of the frequency rotation $s\rightarrow s-j\omega_1$ introduce complex components into the closed-loop transfer function $F(s)$ in (8). These components may produce a different frequency response of $F(j\omega)$ and $F(-j\omega)$, $\omega>0$ since $F^*(j\omega)$ is different from $F(-j\omega)$ (see example in Appendix A) [23].

Moreover, *Example 2* has been included in Appendix A to illustrate the comment in Subsection VI.B.

Comment #11: *As far as the reviewer can see, there is no discussion on the validity of the proposed method in case the system is dq unbalanced as defined in [R1]. Such unbalances are introduced by e.g. PLL, DC-link voltage controller, active/reactive power controllers and synchronous machine saliency. The authors should mention this aspect, or argue if they believe the method is correct even under such unbalances.*

[R1] L. Harnefors, "Modeling of Three-Phase Dynamic Systems Using Complex Transfer Functions and Transfer Matrices," in IEEE Transactions on Industrial Electronics, vol. 54, no. 4, pp. 2239-2248, Aug. 2007.

The MIMO systems are introduced at the end of Subsection II.B and the procedure to address the MIMO system stability from the positive-net-damping stability criterion is commented at the end of Subsection IV.A.2 (see the response to comment #1 of reviewer #2).

Reviewer #4 comments:

Comment #1: *This paper claimed that the main advantage of the proposed alternative positive-net-damping stability criterion over the existing positive-net-damping criterion was that the proposed criterion could provide the frequency of the closed-loop oscillatory modes. However, the reviewer is not convinced by the explanation in this paper.*

#1.a: *The existing positive-net-damping criterion checks the net damping for low frequencies where $|M(jw)N(jw)|>1$, as well as the neighborhood of each open-loop M(jw) and N(jw) resonance, while the proposed criterion checks the net damping in the neighborhood of parallel resonances between the grid and VSC impedance. Both criteria require the impedances of the VSC Yvsc(jw) and the grid Yg(jw) in the full frequency range. According to the comparison presented in Section V-C, it seems that all frequency-domain methods including the impedance-based stability methods are equivalent and they require the same impedance information for stability assessment. The only difference is that these impedance-based stability methods assess the stability from different points of view. Therefore, the reviewer thinks that the proposed criterion is an alternative method but not a method with a significant advantage.*

It is true that all frequency domain methods require the same impedance information for stability assessment and they analyze stability from different points of view. However, the methods have different disadvantages or advantages depending on the point of view. In particular, the proposed approach offers several advantages respect to the impedance-based and positive-net-damping stability criteria because it collects the best of them, i.e., the evaluation of the net damping (more practical than the phase angle between the VSC and the grid admittance ratio) at the parallel resonances between the grid and VSC impedances which provides specific frequencies related with the oscillatory modes and it is easy to characterize. The authors hope that Section V with Fig. 3 and Table II allows clarifying the reviewer concern.

#1.b: *The existing positive-net-damping criterion can still identify the unstable oscillatory resonance frequency as the frequency range where the net damping is negative and $|M(jw)N(jw)|>1$ or as the frequency of each open-loop M(jw) and N(jw) resonance. For example, according to Section V-C, the resonance frequency can be identified in the frequency range between points A and B. Although it may not tell the exact unstable resonance frequency, it can provide the approximate frequency range.*

A comparison between the positive-net-damping stability criterion based on the gain margin condition and the positive-net-damping stability criterion proposed in the paper is made in Section V. The

frequencies characterized from the different conditions and their applications to assess stability are discussed in this Section (see response to comment #4 of reviewer #1).

#1.c: *The proposed method checks the parallel resonances, and the frequency of the parallel resonance with negative net damping is approximately the frequency of the closed-loop oscillatory mode. The frequencies of parallel resonances are determined by Yvsc(jw) and Yg(jw), which is not specifically revealed by the proposed method*

The reviewer concern has been discussed in Section V (see response to comment #4 of reviewer #1). The authors hope that it clarifies this issue.

Also note that the frequency of the parallel resonance between the grid and the VSC admittances is identified in Fig. 6(b) and Fig. 7(b) with the parallel equivalent impedance $Z_t(j\omega)$ (defined in (7)). Considering the frequency response of the grid and the VSC admittances as (16), this parallel resonance can be obtained as (20) or it can also be obtained from the parallel equivalent impedance,

$$\mathrm{Im}\{Z_t(j\omega)\} = \mathrm{Im}\left\{\frac{G_g(\omega)+G_{vsc}(\omega)-j(B_g(\omega)+B_{vsc}(\omega))}{(G_g(\omega)+G_{vsc}(\omega))^2+(B_g(\omega)+B_{vsc}(\omega))^2}\right\}=0 \quad \text{(R16)}$$

$$\Rightarrow \quad B_g(\omega)+B_{vsc}(\omega)\approx 0.$$

The resonance of the grid and VSC admittances (i.e., $\mathrm{Im}\{1/Y_g(j\omega)\} \approx B_g(\omega) = 0$ and $\mathrm{Im}\{Y_{vsc}(j\omega)\} \approx B_{vsc}(\omega) = 0$ in (36)) may not match with (20) or (R16).

Comment #2: *There are some concerns about the derivation of the proposed method*

#2.a: *In Section IV-A-2, the derivation is based on the assumption that the grid and VSC are mainly inductive or capacitive. However, this assumption is mainly true for the high frequency range above the VSC controller bandwidth. Is this derivation also true for the instability caused by the interactions of control loops of multiple VSCs?*

As the reviewer comment, the assumption about the grid and VSC impedance behavior is true at frequencies of the harmonic resonance instabilities (see response to the editor's comment #1). The assumptions of the study are also true independently of the VSCs connected in the system. A short sentence about this issue has been written in the presentation of the Section VI to explain the influence of multiple VSC connection on stability and the validity of the stability methods in these cases:

This application is an example of a grid with multiple VSCs. The connection of multiple VSCs may affect the frequency response of the grid changing the frequency range of its capacitive behavior (i.e., changing the frequency of the parallel resonances) and it may also affect the damping of the grid because the non-passive response of the connected VSCs at the studied frequencies may reduce the grid damping and worsen system stability. However, the above influence does not affect the stability approaches and the assumptions of these approaches as it can be verified in the next Subsections.

#2.b: *In Section IV-B, the admittance Yvsc(s) of the VSC is approximated as 1/(Rvsc + Lvsc*s). Due to the impact of the VSC controller loop, Rvsc might not be always positive. Therefore, the analysis regarding Equation (29) might not be correct.*

The result of the damping stability condition is according with the pole stability criterion in (33) although the VSC resistance R_{vsc} may be negative. A sentence has been written at the end of

Subsection IV.B to illustrate the relation between the damping condition of the positive-net-damping stability criterion and the pole stability criterion:

It can be observed in (32) that a negative VSC resistance R_{vsc} may lead to a positive real part of the poles if $|R_{vsc}| > |R_g|$ (i.e., to a system instability) which is correctly predicted with the negative value of the net damping $G_g(\omega) + G_{vsc}(\omega)$ in (33).

Comment #3: *There are some typos as follows. A proofread of the manuscript is suggested.*

(1) In Line 10 on Page 5, "1+L(s)=Yg(s) + Yvsc(s)" is not correct.
(2) In Line 45 on Page 12, Zt(jw) is not defined.
(3) In Line 15 on Page 15, the positions of "inductive" and "capacitive" should be exchanged.
(4) Equation (30) on Page 11 overlooked the Zcm connected to WT51.

The manuscript has been reviewed and the corrections of the above issues have been made.

Comment #4: *Some details are needed to avoid confusion*

#4.a: *It is better to provide the detailed parameters of the system in Section V, including the physical and controller parameters of the WTs and the line parameters.*

The VSC control data and the WPP data are provided in Table I and Table III, respectively.

#4.b: *It is better to describe the resonance frequency in the unstable case presented in Fig. 5.*

The authors apologise but they do not understand the reviewer comment. The resonance frequency is described in the paper for the stable and unstable cases. A sentence indicating that these parallel resonances are due to the interaction between the inductive behavior of the VSC and the capacitive behavior of the grid has been included in the example:

These resonances are caused from the interaction between the inductive behavior of the VSC and the capacitive behavior of the grid at these frequencies. The cause of the instability is a damping reduction in the VSC contribution because the boundary frequency of the negative damping region is decreased from 1496 Hz to 1381 Hz due to the low-pass filter bandwidth decrease [22].

However, the authors fear that this is not the aim of the reviewer comment. In this case, they are willing to modify the parallel resonance presentation if the reviewer considers necessary.

#4.c: *In Section V-B, are the changes of the feedforward low-pass filter bandwidth and filter inductance for all WTs or just for WT51?*

The changes are made just for WT_{51}. It has been indicated in the example:

The WP stability is analyzed from WT_{51} (see Fig. 4(b)) when the parameters $f_f = \alpha_f/(2\pi)$ and L_f of this WT are modified.

#4.d: *In Line 47 on Page 6, why do "they not provide a clear relation"? What is the "clear relation" revealed by the proposed method?.*

The positive-net-damping stability criterion derived from the gain margin condition does not have a clear relation between electrical resonances of the grid-converter VSC systems and stability because this criterion provides a range of frequencies instead a specific frequency for analyzing stability. This issue has been discussed in the Section V (see response to comment #4 of reviewer #1). The authors hope that it clarifies this concern.

Reviewer #5 comments:

Comment #1: *What's the difference between the passivity mentioned in [10], and the positive-net-criterion mentioned in [15]?*

The authors hope that the comments in Section V clarify this issue:

Among these methods, the passivity-based method imposes passivity in each subsystem (i.e., $G_g(\omega) > 0$ and $G_{vsc}(\omega) > 0$, (16)) for ensuring the closed-loop system stability while the other three methods are less restrictive and do not impose this passivity condition because consider the contribution of each subsystem to stability assessment. As an example, the positive-net-damping stability criterion ensures the closed-loop system stability if $G_g(\omega) + G_{vsc}(\omega) > 0$ (24), and therefore a system could be stable even when VSCs are not passive (i.e., even with $G_{vsc}(\omega) < 0$) if apply $G_g(\omega) > 0$ and $|G_g(\omega)| > |G_{vsc}(\omega)|$.

Comment #2: *What is the exact expression of traditional positive-net damping criterion, and what's the equation of the new positive-net damping criterion?*

The authors hope that Fig. 3 clarifies the reviewer concern. Note that both methods evaluate the net damping $G(\omega)$ (24) at different frequencies. The traditional positive-net-damping stability criterion at the frequencies of the open-loop resonances ($\mathrm{Im}\{1/Y_g(j\omega)\} \approx 0$ and $\mathrm{Im}\{Y_{vsc}(j\omega)\} \approx 0$) and the loop gain greater than 1 ($|Y_{vsc}(j\omega)/Y_g(j\omega)| > 1$). The proposed positive-net-damping stability criterion at the frequencies of the parallel resonances between the grid and VSC impedances ($\mathrm{Im}\{Y_g(j\omega) + Y_{vsc}(j\omega)\} \approx 0$).

Comment #3: *The equation (11) seems inaccurate, since the left hand side is a complex number.*

As it is commented in the response to comment #4 of reviewer #3, this issue has been clarified below (13):

Note that the $M(j\omega)N(j\omega)$ value at the frequency of (12) is the cross point of the Nyquist curve $L(s)$ with the real axis which should be on the right hand side of -1 for stability assessment, i.e. (13) may be hold.

References:

[R1] L. Harnefors, X. Wang, A. G. Yepes, and F. Blaabjerg, "Passivity-based stability assessment of grid-connected VSCs – An overview," *IEEE Journal and Selected Topics in Power Electronics*, vol. 4, no. 1, pp. 116–125, March 2016.

[R2] M. Céspedes and J. Sun, "Impedance shaping of three-phase grid parallel voltage-source converters," 27th Annual IEEE Applied Power Electronics Conference and Exposition (APEC 2012), Feb. 2012, pp. 754–760.

[R3] M. Céspedes and J. Sun, "Mitigation of inverter-grid harmonic resonance by narrow-band damping," *IEEE Journal of Emerging and Selecting Topics in Power Electronics*, vol. 2, no. 4, pp. 1024–1031, Dec. 2014.

[R4] B. Wen, D. Boroyevich, R. Burgos, P. Mattavelli and Z. Shen, "Analysis of D-Q Small-Signal Impedance of Grid-Tied Inverters," *IEEE Transactions on Power Electronics*, vol. 31, no. 1, pp. 675-687, Jan. 2016.

[R5] B. Wen, D. Boroyevich, R. Burgos, P. Mattavelli and Z. Shen, "Small-signal stability analysis of three-phase AC systems in the presence of constant power loads based on measurements d-q frame impedances,"*IEEE Transactions on Power Electronics*, vol. 30, no. 10, pp. 5952-5963, Oct. 2015.

[R6] L. Sainz, Ll. Monjo, J. Pedra, M. Cheah-Mane, J. Liang and O. Gomis-Bellmunt, "Effect of Wind Turbine Converter Control on Wind Power Plant Harmonic Response and Resonances," *IET Electric Power Applications*, doi: 10.1049/iet-epa.2016.0241.

[R7] X. Wang, F. Blaabjerg and W. Wu, "Modeling and analysis of harmonic stability in an AC power electronics-based power systems," *IEEE Transactions on Power Electronics,* vol. 29, no. 12, pp. 6421-6432, Dec. 2014.

[R8] C. Zhang, M. Molinas and A. Rygg, "Properties and Physical Interpretation of the Dynamic Interactions between Voltage Source Converters and Grid: Electrical Oscillation and Its Stability Control," *IET Power Electronics*, early access, http://dx.doi.org/10.1049/iet-pel.2016.0475.

[R9] L. Harnefors, "Modeling of Three-Phase Dynamic Systems Using Complex Transfer Functions and Transfer Matrices," *IEEE Transactions on Industrial Electronics,* vol. 54, no. 4, pp. 2239-2248, Aug. 2007.

[R10] M. Zhao, X. Yuang, J. Hu. and Y. Yan, "Voltage dynamics of current control time-scale in a VSC-connected weak grid," *IEEE Transactions on Power Systems*, vol. 31, no. 4, pp. 2925-2937, July 2016.

[R11] A. Emani-Naeni and R. L. Kosut, "The Generalized Nyquist criterion and robustness margins with applications," *Proc. of the IEEE Conf. on Decision and Control*, Dec. 2012, pp. 226-231.

[R12] R. Burgos, D. Boroyevich, F. Wang, K. Karimi and G. Francis, "On the ac stability of high power factor three-phase rectifiers," *Proc. of the IEEE Energy Conversion Congress and Exposition (ECCE 2010)*, Sept. 2010, pp. 2047-2054.